PHOTOLUMINESCENE AND SIMS INVESTIGATION ON THE DYNAMICS OF NATIVE DEFECTS IN ZINC OXIDE

BY

ZHIYU PENG

THESIS

Submitted in partial fulfillment of the requirements
for the degree of Master of Science in Chemical Engineering
in the Graduate College of the
University of Illinois at Urbana-Champaign, 2018

Urbana, Illinois

Adviser:

Professor Edmund G. Seebauer

Abstract

The technological usefulness of metal oxide often depends upon the behaviors of the defects it contains. Even small differences in defects concentration and distribution will cause significant differences in the electric and optical properties of semiconductor. Defect engineering is aiming at control the semiconductors properties through defect manipulation. The technologies involve controlling defect behaviors by defects types, concentrations, mobility and special distribution. However, beside the Si based system, the applications of defect engineering are less popular.

Controlling the bulk defects via surface chemical states is a relatively new area. Surface offers efficient pathways for point defects creation and annihilation. Due to the lower coordination of the surface atoms requiring less bond creation and breakage, the activation barrier for atoms next for near surface pathways are lower than bulk. The present work uses isotopic gas-solid exchange technology to discover the diffusion-reaction network of oxygen and zinc interstitial in ZnO single crystal.

Simultaneous oxygen and zinc thermal injection through the polar Zn-terminated ZnO (0001) surface showed that the injection of Zn_i stagnate the O_i injection but not by simple site-blocking mechanism.

Room temperature photoluminescence illustrate a new possible defect network that involve the non-excluded H_2 in zinc oxide. Preliminary results show a possibility that the residual hydrogen in ZnO can play important roles in the green-red emission of ZnO single crystal. Accompany with SIMS profile, we believe Zn_i stagnate O_i diffusion by forming non-emissive intermediates.

Acknowledgements

I would like to give the foremost appreciation to my adviser Dr. Edmund G. Seebauer for his patient education, constructive guidance, and encouragements through my graduate school experience. I cannot thank him enough for all the understanding and support he provided. It's my luck to be educated and mentored by him in my academic and real life.

I would like to thank former and current group members Dr. Ming Li, Dr D. Eitan Barlaz, Dr. Kandis Leslie Gilliard, Qilong Huang, Jillian Kuang, and Heonjae Jeong for their constructive advice throughout my academic life at graduate school. I appreciate about their effort to make the lab like a warm home.

I also want to thank to Julio Soares for training and help interpreting Room Temperature PL and PLE data, Timothy P. Spila for TOF-SIMS, and Richard T Haasch on XPS. Without their help, I can't do that. My appreciation also goes to Mike Harland for helping on trouble shooting and maintaining my instruments.

Lastly, I would like to thank my parents and my grandparents. Thank you for supporting all the decisions I made during the past years.

Table of Contents

Chapter 1: Introduction

1.1 Motivation

In ceramic oxide semiconductors, atomic defects such as vacancies, interstitials, and anti-sites can affect the performance of optoelectronic devices [1], sensors [2-4], catalysts [5,6], photo-catalysts [7,8], and photovoltaic cells [9]. To control the behaviors of defects, methods to influence the defect types, concentration spatial distribution, and mobility in solid are essential. Examples of longstanding defect engineering methods in Si based systems [10-12] involve specially designed heating protocol (time, maximum temperature, heating and cooling rates), introduction of foreign atoms, ion bombardment, and amorphization/recrystallization. However, apart from the Si based system, the application of defect engineering is uncommon, with efforts focused mainly on photocatalysts synthesized from metal oxides [13-15].

Controlling the bulk defects via surface chemical states is a relatively new area for defect engineering. Surface offers efficient pathways for point defect creation because fewer bonds need to break than in the bulk structure. This property of surfaces provides a promising route for manipulation of bulk defects. It has been proved that gas-phase injection of oxygen into metal oxides through a clean surface can effectively annihilate the oxygen vacancies in the deep bulk of both TiO_2 and ZnO [16-18]. The high efficiency of O_i injection even can supplant oxygen vacancies as the dominant O-related defects [17-19].

Previous work in TiO_2 highlights the combined roles of surfaces and extended defects in controlling point defect behavior in the deep bulk [18]. An understanding of this interplay points to new strategies for manipulating bulk defects based upon defect reaction

mechanisms that had remained unknown until now. Although substantial progress has been made in understanding the reaction mechanisms including oxygen and the Zn cation in ZnO [17], the results are largely based on the diffusion behavior of O_i only. Independent manipulation of O and Zn defects has not been employed. The present thesis advances the understanding of cation and anion co-diffusion mechanisms by employing an isotopic gas-solid exchange experimental protocol. The thesis demonstrates different reaction and diffusion behavior of the cation and anion compared to TiO_2 [18]. Photoluminescence measurements in oxygen and zinc injected samples give evidence that unintentionally incorporated extrinsic hydrogen [20-21] plays a significant role in that network.

1.2 Outline

The thesis is organized as the following: Chapter 2 discusses the equipment setup and experimental protocol. Chapter 3 focuses on analysis of the diffusion profiles of O and Zn in response to isotopic exchange as measured by secondary ion mass spectrometry. Chapter 4 details the photoluminescence behavior of O and Zn injected ZnO.

1.3 References

[1] H. Kressel, *Semiconductor Semimetals* **16** (1981), 1-52

[2] G. Zhang *et al.*, Sens. Actuator B-Chem. **10** (2000), 144-152

[3] L. Schmidt-Mende *et al.*, Materialstoday **10** (2007), 40-48

[4] P. S. Wijewarnasuriya *et al.*, J. Elec. Mater. **28** (1999), 649-653

[5] M. Casas-Cabanas *et al*., Chem. Mater. **21** (2009), 1939-1947

[6] D. Chen, J. Phys. Chem. C *et al*., **118** (2014), 15300-15307

[7] L. G. Devi *et al.*, Cata. Commun. **10** (2009), 794-798

[8] F. Zuo *et al*., J. Am. Chem. Soc. **132** (2010), 11856-11857

[9] J. M. Azpiroz *et al*., Energy Environ. Sci. **8** (2015), 2118-2127

[10] S. Riepe *et al*., Phys. States. Solidi. C **8** (2011), 733-738

[11] G. Lindstrom *et al*., Nucl. Instrum. Methods Phys. Res **465** (2001), 60-69

[12] L. T. Canham, *Appl. Phys. Lett.* **57** (1990), 1046

[13] M. K. Nowotny *et al*., J. Phys. Chem. C **112** (2008), 5275-5300

[14] T. Takata *et al*., J. Phys. Chem. C **113** (2009), 19386-19388

[15] X. Pan *et al.*, Nanoscale. **5** (2013), 3601-3614

[16] A. G. Hollister *et al*., Applied Physics Letters. **102** (2013) 231601

[17] M. Li *et al.*, J. Phys. Chem. **122** (2018), 2127-2136

[18] K Leslie *et al.*, J. Phys.: Condens. Matter **29** (2017), 445002

[19] P. Gorai *et al*., Appl. Phys. Lett. **108** (2016), 241603

[20] A. Janotti, and C. G. Van de Walle, Rep. Prog. Phys. **72** (2009)

[21] R. Helbig, J. Cryst. Growth **15** (1972), 25

Chapter 2: Introduction of Isotopic Zinc into ZnO Single Crystals: Comparison of Epitaxial Growth and Direct Injection Approaches

2.1 Introduction

Controlling the bulk defects via surface chemical states is a relatively new area for defect engineering. Surface offers efficient pathways for point defects creation because fewer bonds need to break than bulk structure [1]. This property of surface provides a promising route for manipulation of bulk defects. Gas-solid experiments have been proven as an effective method on examination the anion self-diffusion behaviors in metal-oxide [1-4]. However, examination of cation self-diffusion by gas-solid exchange experiment is much harder as the metal cation more likely comes into the surface via metallic form instead of gaseous, and it may more likely to condense on the surface. The other methods such as ion implantation [5-7] may not be applied as the implanted ion can induce near-surface lattice damage [8] which can affect self-diffusion of defects. To avoid this problem, alternative methods such as epitaxially grown isotopic heterojunction structures [9-11] and continuous isotopic cation flux injection [12-14] are widely used. After attempts at both epitaxial growth and direct flux injection methods for Zn injection in ZnO (0001) single crystal, the epitaxial growth method was ruled out since a high quality epilayer of ZnO was hard to grow.

2.2 Epitaxial Growth Approach

The isotopic heterojunction approach have been widely used in other semiconductor systems such as Si [15-17], TiO_2 [18], and Ceria [19]. The main idea behind the epitaxial growth approach is epitaxial growth of a thin layer (eg. 10 nm) of ZnO with isotopically labeled zinc

and labeled oxygen elements on a pre-annealed natural abundance ZnO single crystal. Growth is followed by annealing under a controlled natural abundant oxygen atmosphere and temperature to avoid non-stoichiometry of the substrate surface due to the oxygen loss during post annealing. Then isotopic depth profiles of both the cation and anion are collected by ex-situ by secondary ion mass spectroscopy (SIMS). Figure 2.8 shows a schematic of the defects exchange network for the isotopic heterojunction.

Due to the properties of high quality thin epi-layer should same as the surface of single crystal substrate, isotope diffusion study through epi-layer should tell the exact behaviors of defects. The modeling for this method should be simpler because it avoids the problems cause by surface reconstruction or so. Furthermore, most of the existing models are developed under the single crystal bulk condition, which can be easily modified and applied to the system here. The most challenging part of this method is the growing of the high quality of epi-layer in high level. Any formation of line defects or extraneous intrinsic and extrinsic point defects will largely affect the diffusion mechanisms. To make the diffusion measurements reflect true single crystal behavior, grain boundaries should not be observed in the epi-layer.

2.2.1 Experimental Method and Setup

For financial issues, the growing ZnO layer on Si(100) wafer was tested initially. Figure 2.1 shows a schematic of the chamber setup for the experiment. The base pressure of the chamber can reach 3×10^{-8} torr with overnight pumping. It need to indicate that as a type of volatile metal, Zn has extremely high vapor pressure under low temperature. To avoid potential loss and oxidation of the metal in vaporization source, the chamber should not

conduct long time high temperature baking. The Si(100) substrates (roughly in dimensions of 1cm×0.5cm×0.1cm) were degreased by 5 mins ultrasonic baths in acetone, isopropyl alcohol, and methanol consecutively before mounting into the UHV chamber. To minimize the surface contamination, the total ambient exposure time for substrates were limited to less than 30 mins.

Prior to growing, the substrate is pre-annealed in UHV environment in 650 °C for 30 mins to remove surface contamination of carbon and nitrogen. The Zn flux was supplied by evaporating 4N-purity Zn metal from a conventional Knudsen cell with BN crucible and heated by contact with a tungsten filament coil. The Zn flux was monitored by cell temperature via Chromel-Alumel thermocouple and beam equivalent pressure (BEP) via a nude cathode ion gauge that placed between the cell and substrate. For long term run under oxygen environment, BN crucible is not suggested due to, at high temperature (900 °C above), BN can react with oxygen to produce B_2O_3 (**Equation 2.1**), which has porous structure with high vapor pressure [20,21]. For the experiment conditions used here, B_2O_3 should not cause too many problems.

$$4BN + 7O_2 \Leftrightarrow 2B_2O_3 + 4NO_2 \qquad (2.1)$$

Most of the Knudsen cell design was inherited from previous group member [22]. Figure 2.2 shows the schematic of the cell. One improvement is the cell cap, here a counterbore was drilled on the cell cap to get better control of Zinc flux without sacrificing the efficiency of the Knudsen Cell [23-25]. In addition, due to the BN is too fragile to drill threads in it, the 0-80 set screws that were used in place of ceramic adhesives to hold the caps to the crucibles were substituted by two stainless rods with same diameter.

Lastly, it found that during the experiments, a large portion of Zn metal would aggregate on the inner side of cap regardless whether under oxygen environment or not. It was believed that cell temperature was not distributed uniformly and drop dramatically near the cap. To make a more controllable diffusion apparatus, a Macor thermal shield was created by SCS Machine Shop were used here. It resulted no further metal aggregation in the following experiments. Figure 2.3 shows the schematic of the Macor thermal shield. All the units in the figure are in inches.

During growing, the 5×10^{-5} torr natural abundant O_2 gas was supplied in the chamber. The Knudsen cell was kept at 200±1 °C during the growing process for stable Zn beam supply. Before supplying oxygen gas, the substrate was exposed to Zn flux for 5 minutes to introduce an initial Zn layer. In order to optimize crystal perfection and surface morphology, the substrate temperature were varied from 400 °C to 650 °C. Growing processes lasted 30 mins for each temperature point. Then the specimens were tested by ex-situ XPS to determine the qualities of the film.

2.2.2 Results and Discussion

Figure 2.4 shows XPS data for samples treated under different temperatures. None of the as-grown samples showed a sharp $Zn2p_{3/2}$ peak at 1022 eV [26], and only the 400 °C sample showed a tiny peak there. This result supports the point that the high dissociation energy of O_2 (5.16 eV) [27] hindered the thermal dissociation process on substrate surface. Furthermore, Zn metal is a type of "volatile metal", and it has relatively high vapor pressure at low temperature (the melting point of Zn metal is 419.5 °C). Hence, in the experimental environment, Zn metal may re-evaporate from the substrate surface very quickly, which

further hinders the slow oxidation process on the substrate surface. The assumption in agreement with the existing literature, which showed that the epitaxial growth rate of ZnO dramatically drops above 350 °C [28].

Instead of thermal cracking oxygen gases, alternative reactive oxygen sources were widely applied in MBE and PLD application [28-31]. Among the alternative sources, RF (radio frequency) plasma or radical sources are widely used. ECR (electron cyclotron resonance) sources, simple ozone and hydrogen-peroxide sources have been used as well. Although oxygen plasma is widely preferred in MBE applications, this technology has the disadvantages of oxidation of source material and possible surface damage by high-energy particles, which increases the concentration of oxygen vacancies in the substrate [32]. The alternate sources such as nitrogen dioxide, ozone, hydrogen peroxide may have less of those problems [29].

After comparing those candidates from nitrogen dioxide to hydrogen peroxide, hydrogen peroxide was picked as, without extra contamination like nitrogen, it's easier to handle with the current vacuum system. Most the setup was kept similar to previous, except the oxygen source was substituted by a H_2O_2 jet-line. The schematic of the setup was shown as Figure 2.5. The distance from the substrate to end of H_2O_2 nozzle was about 4 cm, and the nozzle diameter was around 0.2 cm. To increase the purity of the H_2O_2 in the H_2O_2 gas line, a gas handling system setup was applied. Figure 2.6 is the schematic of the setup. This setup resembled that of a previous group member [22], but was much simpler. During the growing, the H_2O_2 vessel was heated by a 90 °C water bath to increase the H_2O_2 partial pressure in the gas line. During H_2O_2 jet introduction, the mechanical pump for the gas handling system was turned on. The remaining experimental protocols were kept same as described in the previous chapter.

The XPS results are shown in Figure 2.7. It showed the similar results as the sample prepared under pure oxygen environment. The new samples showed clearer and sharper $Zn2p_{3/2}$ and $Zn2p_{1/2}$ peaks below 650 ºC, but the peaks were still not significant. On the other hand, with increased amount of Zn deposited on the substrate, the samples showed more severe problems with B deposition. With increased growing temperature, the B peak around 188 eV grew significantly. These results recalled the worries about BN crucible that described in previous paragraph. The introduction of H_2O_2 didn't significantly improve the efficiency of ZnO growing, but it caused additional problems (introduction of extra contamination) with current setup. To avoid this problem, the Al_2O_3 crucible can be used as a substitution. However, accompany with the further experimental hardness on growing high quality ZnO epi-layer [1] and the low likelihood for ZnO deposition under pure oxygen environment [16-18], the epitaxial growth approach was abandoned.

2.3 Direct injection Approach

Direct injection approach can be achieved by annealing the natural abundance ZnO single crystal substrate under a controlled isotopic labeled Zn and O_2 pressure. Then the isotopes diffusion profiles are measured by ex-situ SIMS. Figure 2.9 shows a schematic of the defects exchange network for the direct injection approach.

Direct injection method should be easier to achieve experimentally as the only thing we need to bother with is whether a layer of ZnO grows on the substrate. In contrast to the other method, we don't want anything growing on the surface. Any ZnO grow on the surface will increase the difficulty to distinguish the origin of isotope Zn in the diffusion profile, and highly defected ZnO will have unreliable results too. According to the results from epitaxial

growth approach, the ZnO growing should not be a big issue. On the other hand, this method is more amenable to modeling as we could adapt well-developed model, which was built on the other systems, on ZnO.

2.3.1 Experimental Method and Setup

Most of the setup was kept same as the one used in epitaxial growth approach. One exception is we no longer use H_2O_2 as the oxygen source but pure oxygen gas. The experiment applied the well-known isotopic gas-solid exchange protocol to measure the oxygen and Zinc self-diffusion simultaneously. The Zn-terminated ZnO(0001) single crystal (CrysTec) in dimensions of 1cm×0.5cm×0.05cm were degreased in ultrasonic bath by acetone, isopropyl alcohol, and methanol respectively. Each rinse took 5 minutes. To minimize the surface contamination, the total ambient exposure time for substrates were limited to less than 30 min.

Prior to exposing the sample under zinc and oxygen environment, the sample was pre-annealed in natural abundance O_2 environment for 4 hours at different substrate temperature and pressure to equilibrate the bulk defects and thermally clean the substrate surface. The temperature and O_2 pressure were kept same as the ones would use in the isotopes diffusion annealing. After the pre-annealing, the specimens were annealed in $^{18}O_2$ gas (Sigma-Aldrich Inc., ≥97% purity) and ^{67}Zn flux for 105 mins. The ^{67}Zn flux was supplied by the Knudsen cell with isotopic label ^{67}Zn metal (Trace Sciences International, ≥97% purity). During the diffusion annealing, the turbo pump was throttled by a gate valve with about 1/2 closed in order to maintain the desired pressure in the chamber.

The isotopic oxygen and zinc depth profiles were measured ex-situ with TOF SIMS (PHI-TRIFT III) with negative and positive cesium ion beam. The equipment correction factors were calculated and calibrated by measuring the as-received natural abundance ZnO(0001) samples. The detailed SIMS results will be discussed in the Chapter. 3.

2.4 Conclusion

The deposition of isotopically labeled epitaxial heterojunctions was initially used as a protocol for ^{67}Zn and ^{18}O diffusion in the bulk ZnO single crystal. However, the difficulty of growing ZnO epitaxial layers under both O_2 and H_2O_2 environments, and the potential challenges of controlling the point defect concentration inhibit the application of this experimental technique to isotopic tracer diffusion studies. On the other hand, from the epitaxial heterojunction experiments, we found that under O_2 environment, ZnO was unlikely deposited on Si above 500 °C. It offered a window for the direct injection approach, in which we didn't want any undesired adsorbate to poison the clean surface. Thus, epitaxial growth approach was abandoned, and direct injection approach was chosen instead.

2.5 Figures

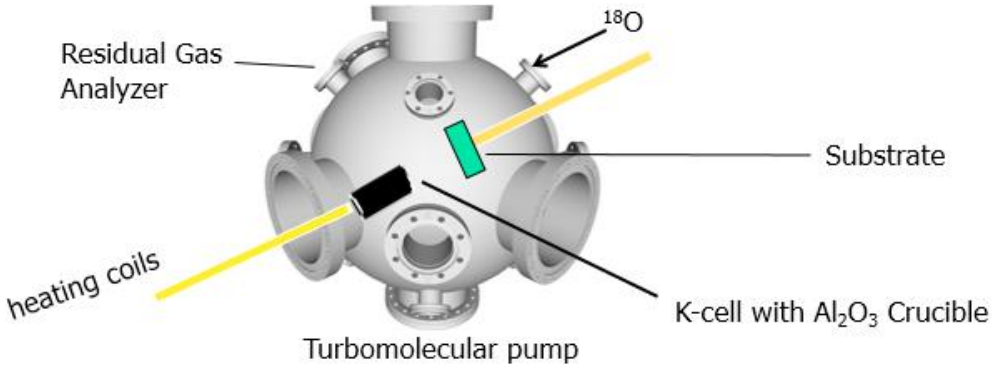

Figure 2.1 Equipment Setup

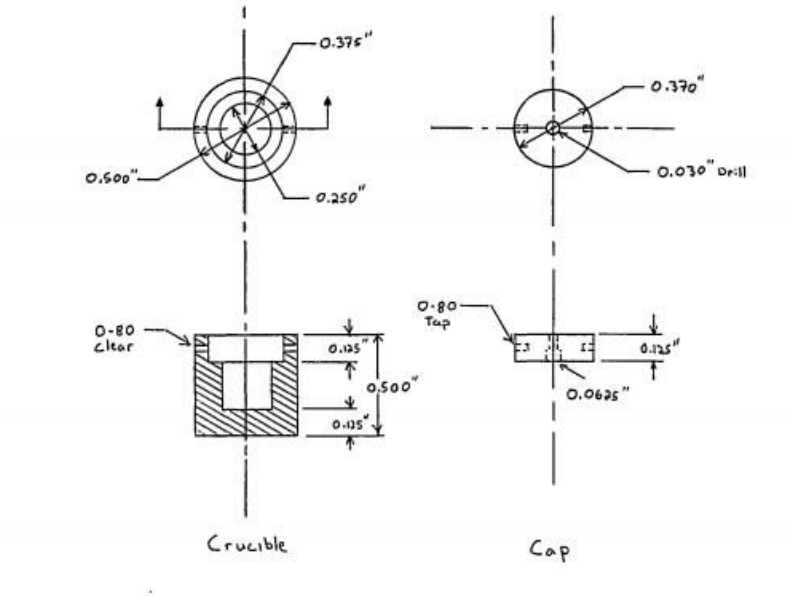

Figure 2.2 Schematic of BN Knudsen Cell

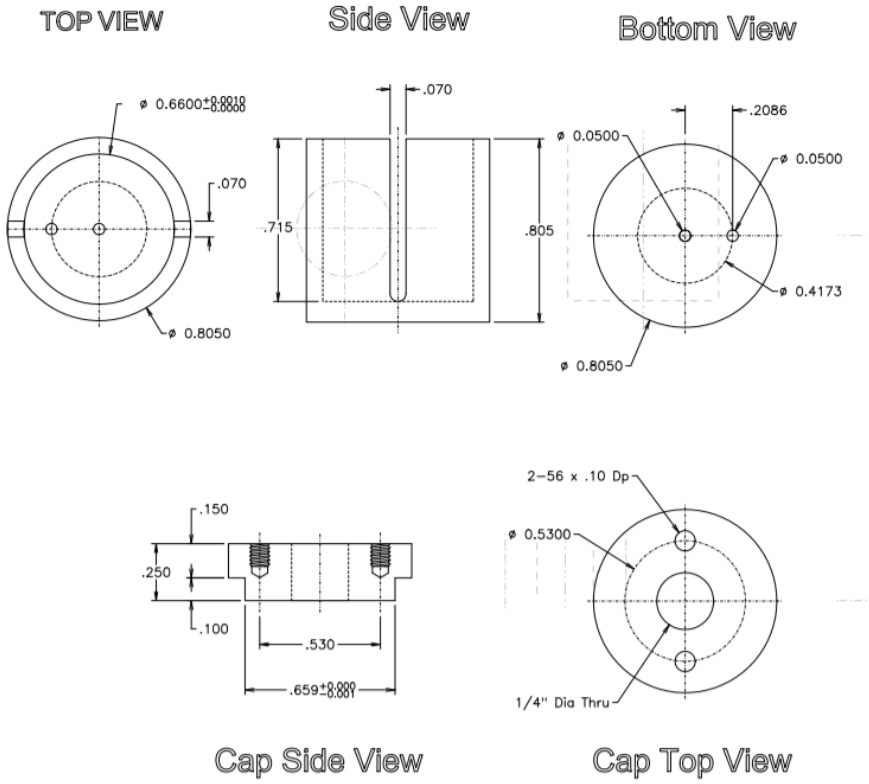

Figure 2.3 Macor thermal shield

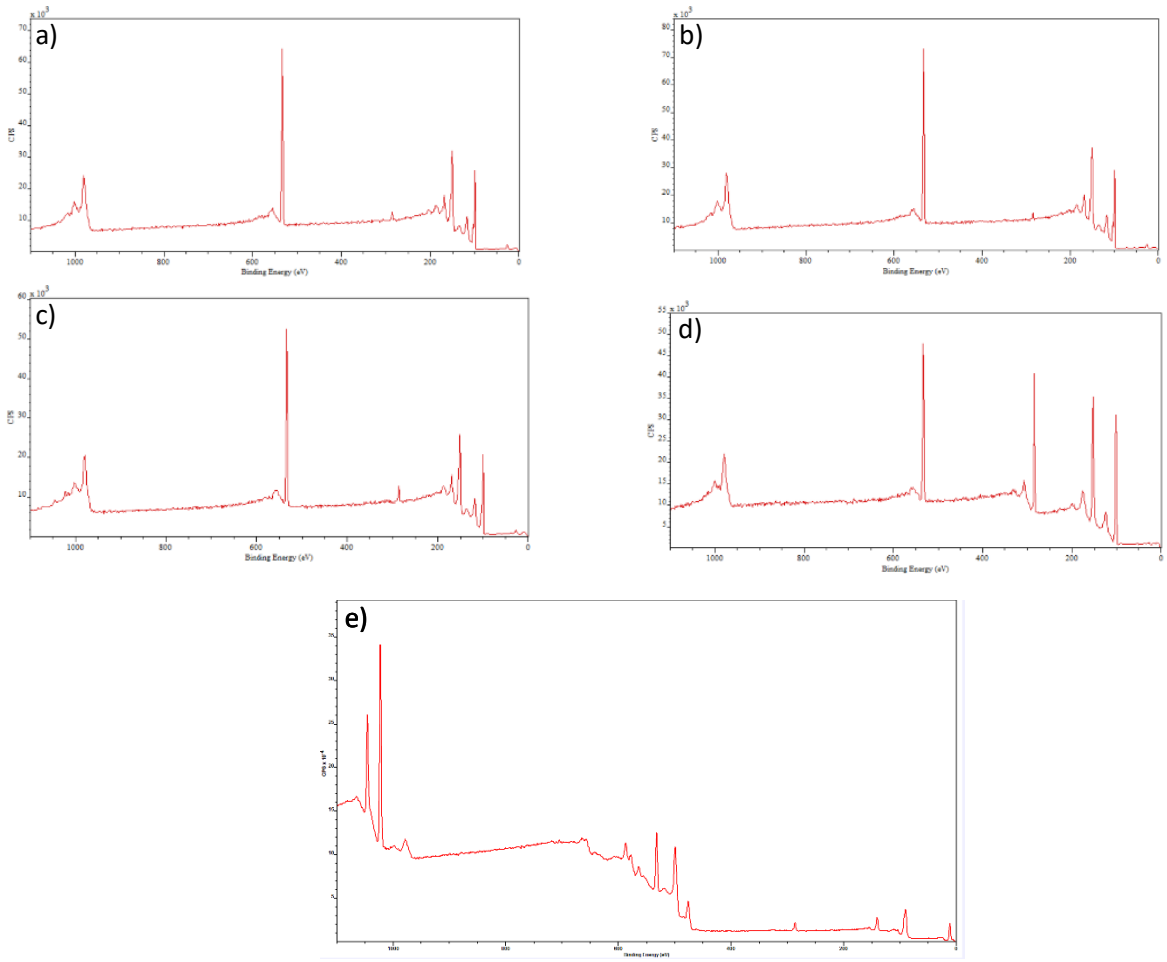

Figure 2.4 XPS profiles for as-grown ZnO on Si(100) substrate by oxygen gas in a)400 °C b)500 °C c)600 °C d)650 °C e) As-receivedZnO (0001) single crystal

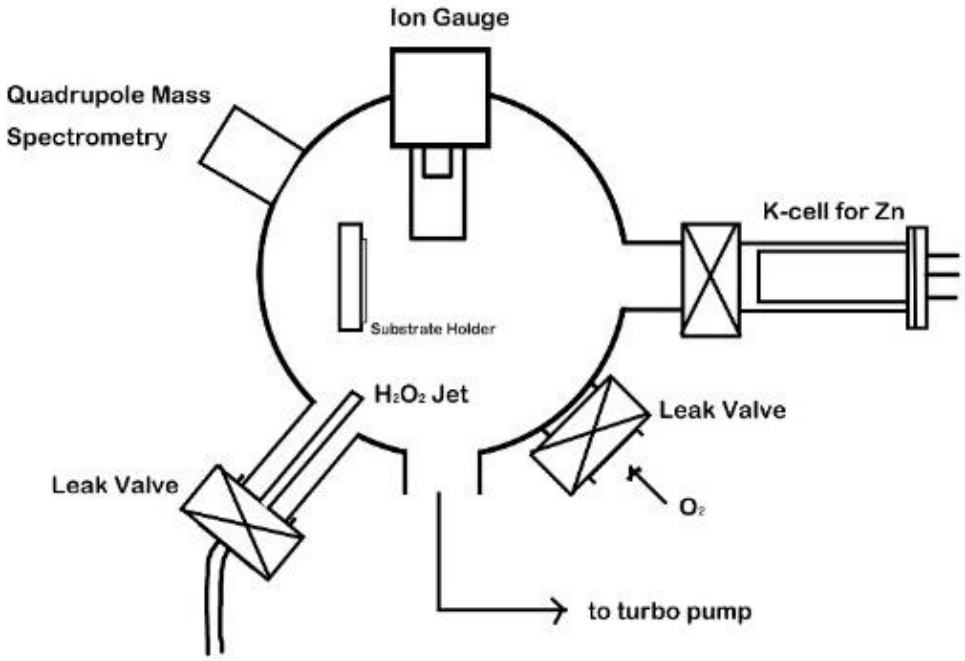

Figure 2.5 Equipment setup for H_2O_2 oxygen source

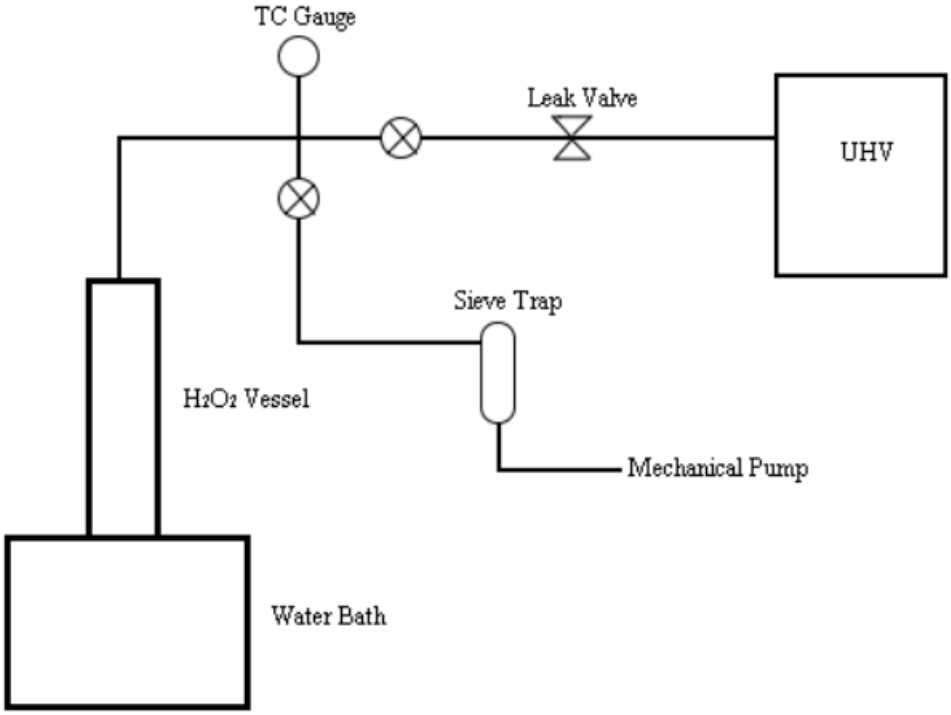

Figure 2.6 Schematic of Gas Handling System

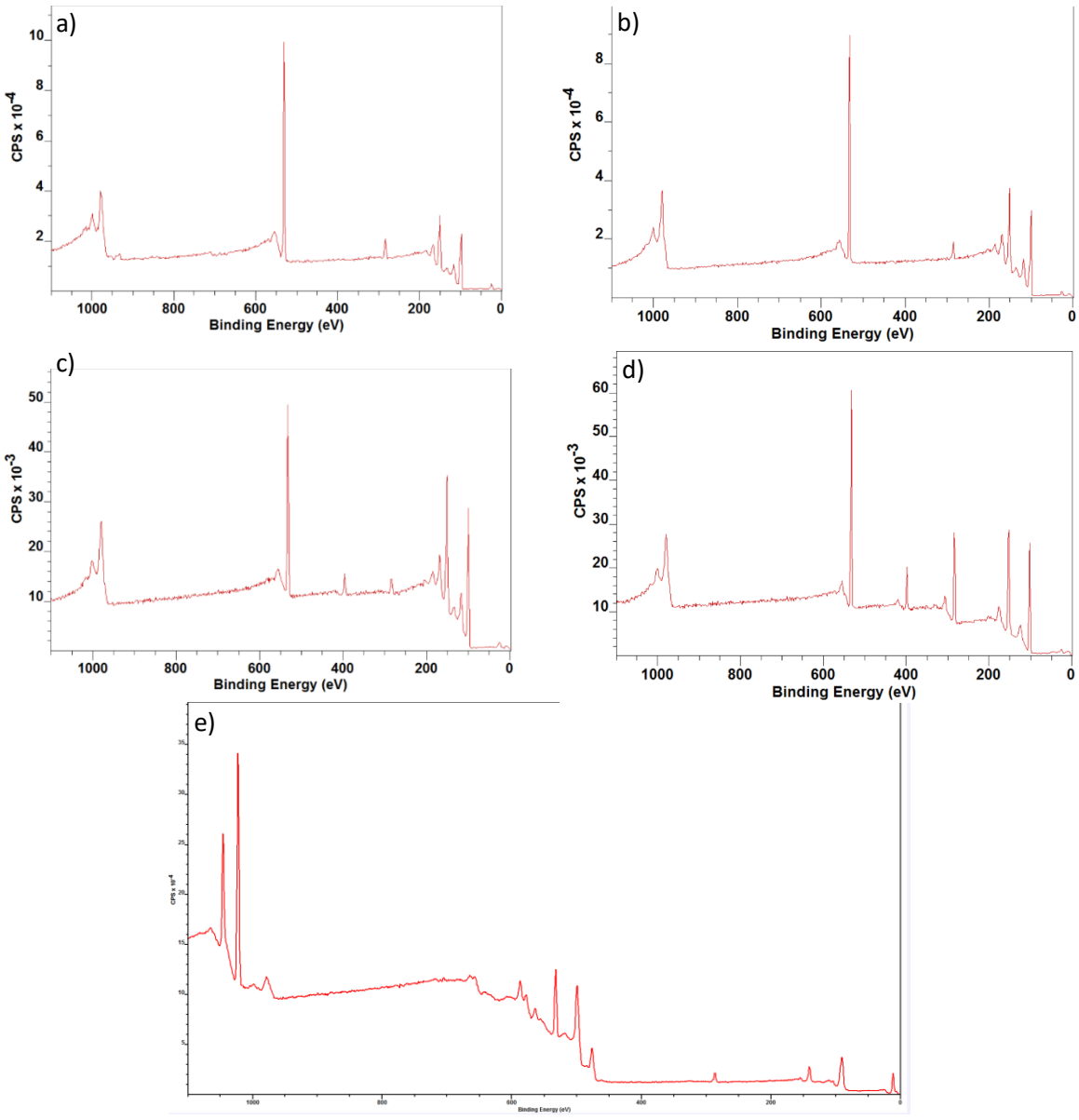

Figure 2.7 XPS profiles for as-grown ZnO on Si(100) substrate by H_2O_2 in a)400 °C b)500 °C c)600 °C d)650 °C e) As-receivedZnO (0001) single crystal

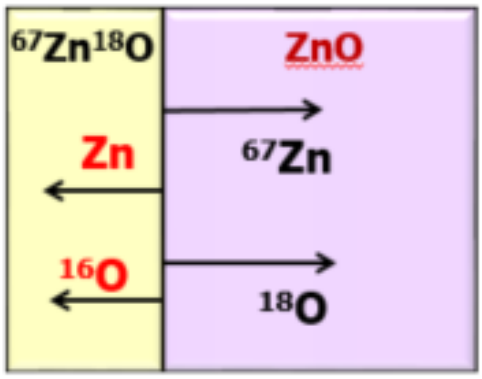

Figure 2.8 Schematic of the defect exchange of the isotopic heterojunction approach

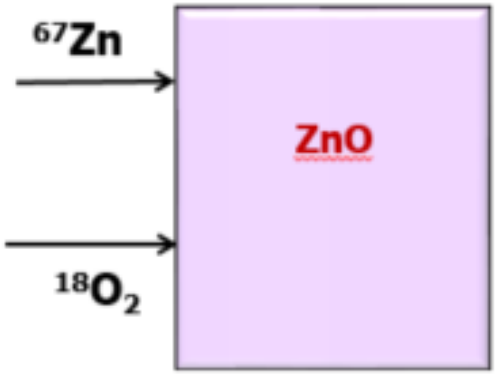

Figure 2.9 Schematic of the defect exchange of the direct injection approach

2.6 References

[1] E. Seebauer *et. al.*, Phys. Rev. Lett. **97**, (2006) 055503

[2] P. Gorai *et. al.*, J. Chem. Phys., **144** (2016) 184708

[3] M. Li *et. al.*, J. Phys. Chem. C, **120** (2016)

[4] K. Gilliard, PhD Thesis (2017)

[5] J. R. Conrad *et. al.*, J. Appl. Phys. **62** (1987)

[6] M.Y.L. Jung *et. al.*, J. Appl. Phys. **97** (2005) 063520

[7] A. Ghicov *et. al.*, Nano Lett. **6(5)** (2006)

[8] A. Gat *et. al.*, Appl. Phys. Lett. **32** (1978)

[9] R. Vaidyanathan *et.al.*, AIChE J. **52(1)** (2006)

[10] HD. Fuchs *et.al.*, Phys. Rev. B **51** (1995)

[11] O. Ambacher *et. al.*, Jpn. J. appl. Phys **37** (1998)

[12] G. W. Tomlins *et. al.*, J. Appl. Phys **87**(1) (2000)

[13] W. J. Moore *et. al.*, Discussions of Faraday Society 7 (1959)

[14] M. Kilo *et. al.*, J. Appl. Phys. **94** (2003)

[15] A. G. Hollister *et. al.*, Appl. Phys. Lett., **102** (2013) 141601

[16] C. T. M. Kwok *et. al.,* J. Appl. Phys. **98**, (2005) 013524

[17] R. Vaidyanathan *et. al.*, AIChE J. **52**, 1 (2006)

[18] K. L. Gilliard, PhD thesis (2017)

[19] C. L. Perkins *et. al.*, J. Vac. Sci. Technol **19** (2001), 1942

[20] Jacobson, Nathan, *et al*. "High Temperature Oxidation of Boron Nitride. Part 1; Monolithic Boron Nitride." (1997)

[21] Lavrenko *et al*, Ceram. Int. **12** (1986), 25-31

[22] Kurt Alan Schultz, PhD Thesis (1992), 37

[23] M.A. Herman, “Molecular Beam Epitaxy: Fundamentals and Current Status.” *Springer Series in Materials Science 7*

[24] A. M. Booth, Atmos. Meas. Tech. **2** (2009), 355-36

[25] Garland, Nibler, and Shoemaker (GNS) (8th ed) pages 119-127, 587-594, and 597

[26] D. R. Lide (Ed.), CRC Handbook of Chemistry and Physics, 79th Edition. CRC Press, Boca Raton, FL, 1998-1999

[27] R. Al-Gaashani *et al.*, Ceramc. Int. **39** (2013), 2283-2292

[28] Y. W. Heo *et al*., Appl. Surf. Sci. **252** (2006), 7442-7448

[29] N. Izyumskaya *et al.*, J. Cryst. Growth **269** (2004), 356-361

[30] X. W. Sun *et al*., J. Appl. Phys. **86** (1999), 408-411

[31] A. Bakin *et al.*, J. Cryst. Growth **287** (2006), 7-11

[32] K. Nakahara *et al*., Jpn. J. Appl. Phys. Part 1 **40** (2000), 250

Chapter 3: SIMS Investigation of Oxygen and Zinc Injected into ZnO (0001) Single Crystals

3.1 Introduction

Surface offers efficient pathways for point defects creation because fewer bonds need to break than bulk structure. This property of surface provides a promising route for manipulation of bulk defects. Atomically clean surface has the highest number of un-bonded orbitals, so it should inject or annihilate point defects faster than the rough surface [1]. It has been reported that clean surface can significant increase the O_i injection in rutile TiO_2 (110) [2], ZnO (0001) [3], and self-diffusion in Si [4]. All the results can point out that the atomic clean surface open a fast path for mobile defects injection and, vice versa, annihilation. This unique method on controlling injection rates of mobile point defects provides a way to control the other point defects in bulk. For example, annihilate V_O by inject O_i.

Recent research in rutile TiO_2 with simultaneously inject O_i and Ti_i showed an interesting result that the extended defects in rutile TiO_2 can act as a sink for O_i [5]. It showed a new potential direction for the defect interaction network. It makes the unknown behaviors of Zn cation injection into the bulk ZnO single crystal more attractive.

3.2 Experiment

The experiment protocol adapted the isotope gas-solid exchange experiment that well-used in the other semiconductor system [5,6]. The detailed experimental setups was introduced in Chapter. 2. The Zn-terminated ZnO (0001) single crystal were bought from CryTec Inc. with dimension of 1cm×0.5cm×0.05cm. Before the mounted the sample into the UHV chamber, to remove the potential organic contaminations, the sample were cleaned by

ultra-sonic bath with acetone, isopropyl alcohol, and methanol respectively. Each rinse took 5 minutes. To minimize the potential contamination from ambient atmosphere, the samples were kept outside of the chamber for less than 30 mins after rinsing.

Before the exposure the samples into isotopic zinc and oxygen flux, the sample was pre-annealed under natural abundance oxygen environment for 4 hours at different temperature (from 540 °C to 600 °C) by a SiO_2/Si backing plate and different pressure (from 1×10^{-5} torr to 1×10^{-4} torr) to equilibrate the bulk defects and thermally clean the substrate surface. Followed by the pre-annealing, the samples were annealed under $^{18}O_2$ gas (Sigma-Aldrich Inc., ≥97% purity) and ^{67}Zn flux (Trace Sciences International, ≥97% purity). The annealing time were 105 mins, and the substrate temperature and $^{18}O_2$ pressure were kept identical as them in pre-annealing procedure. The zinc flux was supplied by vaporizing ^{67}Zn metal by a Knudsen Cell at 200±1°C. Secondary ion mass spectrometer (SIMS) measurements were performed ex-situ by PHI-ToF Secondary Ion mass spectrometer with positive and negative Cs primary ion beam with ion energy equal to 2keV. For each SIMS experiment, a controlled sample (as-received sample) was measured to calibrate the equipment factors of SIMS. The normalization respect to the controlled sample were used to calculate the absolute value of the isotopes.

3.3 Results and Discussion

The isotopic diffusion profiles for the samples annealing under 5×10^{-5} torr oxygen pressure were shown in Figure 3.1 and 3.2. In Figure 3.1, for ^{18}O diffusion profile, except the sample annealing under 600 °C, all samples have the steep near-surface pileup (8-20 nm) of isotope accumulation. The localized pile-up are believed to result from the interaction of

charged defects and the electric field in the near-surface charge region [7]. It has also been proved that the surface charged regions will not affect the near-surface diffusion behaviors of charged defects mathematically [8]. Compared with previous experiments that employed an oxygen-only environment, the oxygen diffusion profile preserved the slowly decayed exponential tail even with exposure of Zinc flux [3]. This shape indicate that the oxygen diffuse via a highly mobile intermediate that occasionally exchanges with the lattice atoms [9]. Hence, for this case with Zn in the gas phase, the oxygen still diffused as O_i that exchange with the lattice by kick-in mechanism. The long exponentially shaped tail indicates that in this specific period, the short time asymptotic limit for oxygen was kept and the identities of the dominant oxygen related diffusion intermediates haven't changed at all [10].

Figure 3.2 also shows some interesting profiles for ^{67}Zn injection. With clear concentration change of ^{67}Zn at different temperature, all profiles showed no surface pile-up regions and exponential tails that decayed into the bulk either slowly or not at all. There has some possible explanations for this profile shape. DFT calculations, in n-type ZnO, indicate that the activation barrier for Zn_i exchange with Zn sites in the lattice is very low (less than 0.6 eV), and this energy is much smaller than the migration barriers for any other types of native defects in ZnO [11-13]. This result agrees with experiments employing optical detection of electron paramagnetic resonance (ODEPR) experiment at different annealing temperature [14].

$^{67}Zn_i$ has opposite charge to O_i. For O_i, the strong electric field in the space charge region (SCR) of ZnO (0001) single crystal can slow down the diffusion of O_i in the SCR. In the isotopic SIMS depth profile, such slowing will manifest as pile-up near the surface [16]. Hence, for Zn_i the same electric field should accelerate its diffusion, and a near-surface valley should

be observed in the isotopic depth profile [16]. However, in this profile, we couldn't see the valley region for $^{67}Zn_i$ (Figure 3.2). The disappearance of the valley at the space charge region (SCR) might suggest the $^{67}Zn_i$ diffused extremely fast and the weak near surface electric fields only had very limited amount of time to drift the $^{67}Zn_i$ diffusion. Thus the valley region may dissolve into the background profile of $^{67}Zn_i$ [5]. Another possibility is that, under the spatial resolution of the SIMS during the experiment, the valley region might be too shallow to be observed.

On the other hand, in agreement with DFT calculations [11-13], it could give us a side-view about the fact that Zn_i diffused much faster than O_i because, with same magnitude of charge state, the surface pile-ups were significant for O_i [5-9] but weak for Zn_i. However, this assumption is true only if the mean diffusion length (for Zn_i) is extremely large, which means it seldom exchanges with the lattice during the diffusion time. Otherwise, in the 105 min annealing interval, the Zn_i may interchange with the lattice several times before O_i does. In that case, the exponential profile for ^{67}Zn will not be kept, but a conventional complementary error function profile instead [7].

However, because the region of depth profiling was much shallower (around 100 nm) than the complete profiles, the Zn profile might still in the near the surface plateau region of a complementary error function. Therefore, we could not tell too many details about the identity of the diffusant by the shape of profile. Due to the availability of SIMS in the past one and a half year, the data available may not have enough information to solve this problem. However, even without a detailed understanding of the zinc-related diffusion mechanism of ZnO, the SIMS data still gives us a clear indication of the notable amount of zinc injection into the bulk structure.

Some important kinetic factors like net injection flux (F), mean diffusion length (λ), and the effective diffusivity (D_{eff}) may be extracted from the diffusion profile by applying the analytical model that was developed by a previous group member [9]. Detailed background will not be given here. Figure 3.3 and Table 3.1 demonstrates the numbers extracted from Figure 3.1. Compared with previous oxygen-only experiments [6], with exposure of ^{67}Zn flux, the ^{18}O net injection flux was about one order of magnitude lower at each temperature point. This result is opposite to the observation of O_i and Ti_i co-diffusion in rutile TiO_2, where the flux of ^{18}O was notable higher than the clean-surface and sulfur adsorbed surface [5].

Furthermore, with ^{67}Zn flux, the mean diffusion length of O_i showed strong and positive correlation to the temperature (Figure. 3.3), and the values were much smaller than the oxygen only samples, which almost kept identical as 6000±500 nm from 510 °C to 600 °C [6]. In contrast, for rutile TiO_2 the mean path length of O_i also showed positive correlation to temperature, but the temperature dependences were much weaker, and, for both O_i and Ti_i, they had similar pre-factors and activation energies to each other [5].

For the diffusion profile of ^{67}Zn, the surface was assumed in quasi-equilibrium with the bulk. However, we could not preclude the possibility that Zn_i might never reach thermal-equilibrium during the pre-annealing and post-annealing procedure as the Zn might slowly be lost into the vacuum, whereas the loss of O was compensated by oxygen background pressure. To solve this problem, the value was calculated using the integrated areas, where had exceeded isotopes, of the depth profiles. However, due to the very horizontal shape of the ^{67}Zn depth profiles, the depth at which the isotope concentration approached the natural abundance level was be a very hard to determine. Here, the total profile depths for ^{67}Zn at

540 °C and 570 °C were estimated by the intersection of the trend line of the ^{67}Zn depth profiles and the natural abundance ^{67}Zn line. For the 600 °C profile, the total profile depth was roughly estimated as 4000 nm. The same method was also used to calculate the value of F in the ^{18}O diffusion profile at 540 °C, where the total profile depths was estimated as 1000 nm. The calculated results were shown in Figure 3.4 and Table 3.1.

In comparison with Ti_i and O_i diffusion in rutile TiO_2, in ZnO the values of λ of Zn_i and O_i were roughly 100 times greater than Ti_i and O_i . In the meantime, the effective diffusivity, of Zn_i and O_i were roughly 1000 times greater than Ti_i and O_i [5]. With such high mobility of O_i and Zn_i in ZnO, we might believe that extended defects might not serve as efficient sources or sinks for O_i and Zn_i. Hence, the extended defects theory in rutile TiO_2 probably does not operate in ZnO (0001).

With clear indications of Zn being injected into the bulk (Figure 3.3), we might conclude that the Zn related defect retard the diffusion of O_i. Due to the greatly decreased mean diffusion length compared with the O_2 only samples [6], the Zn related defects might not affect the O_i injection by simply blocking the effective injection sites of oxygen like sulfur atoms [15]. However, due to the possibility of variance of temperature measurements between my experiments and those of previous group members, comparisons to previous data may not be exact. Although the room temperature photoluminescence of the ^{18}O only samples of mine and previous group member showed exact the same spectra, SIMS measurements on my ^{18}O only sample were essential.

3.4 Conclusion

Simultaneous oxygen and zinc thermal injection through the polar Zn-terminated ZnO (0001) surface was studied using isotopic diffusion experiment. At the studied temperature range, the net injection flux of ^{18}O in zinc injected samples were an order of magnitude less than the samples annealed in O_2 only environment. The significant change of the mean diffusion length of ^{18}O might indicate that the injection of Zn_i stagnate the O_i injection but not by simple site-blocking mechanism. The disappearance of near surface pile-up and flat tail for ^{67}Zn diffusion profiles might suggest that Zn diffuse as an extremely fast moved intermediate.

Although the lack of SIMS data could not give us dominant amount of information about the behaviors of the zinc-related defects, the preliminary data showed that Zn can be thermally injected into the bulk and reiterated the importance of clean surface for injection Zn_i.

3.5 Figures and Table

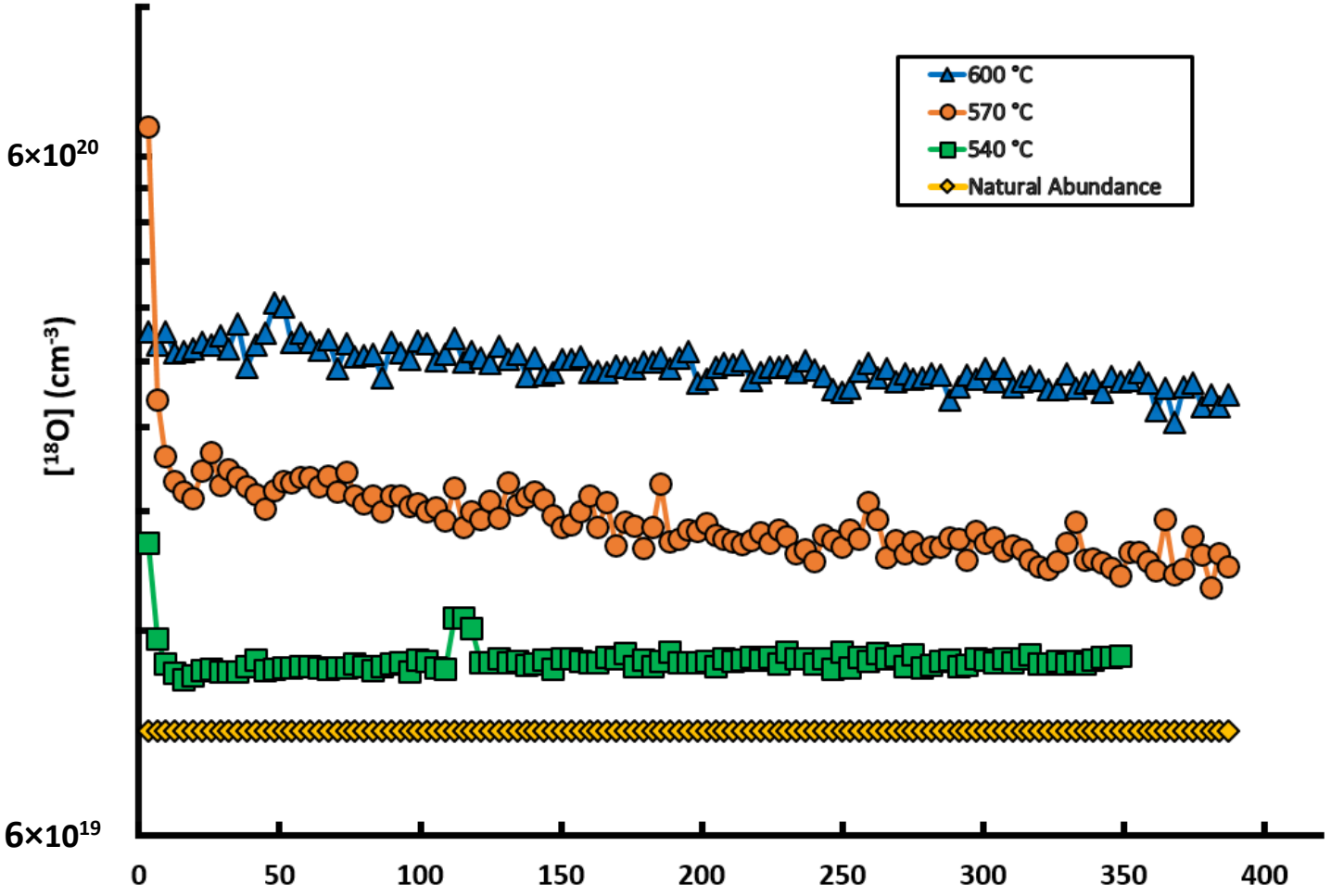

Figure 3.1 ^{18}O Diffusion Profile at oxygen pressure of 5×10^{-5} torr

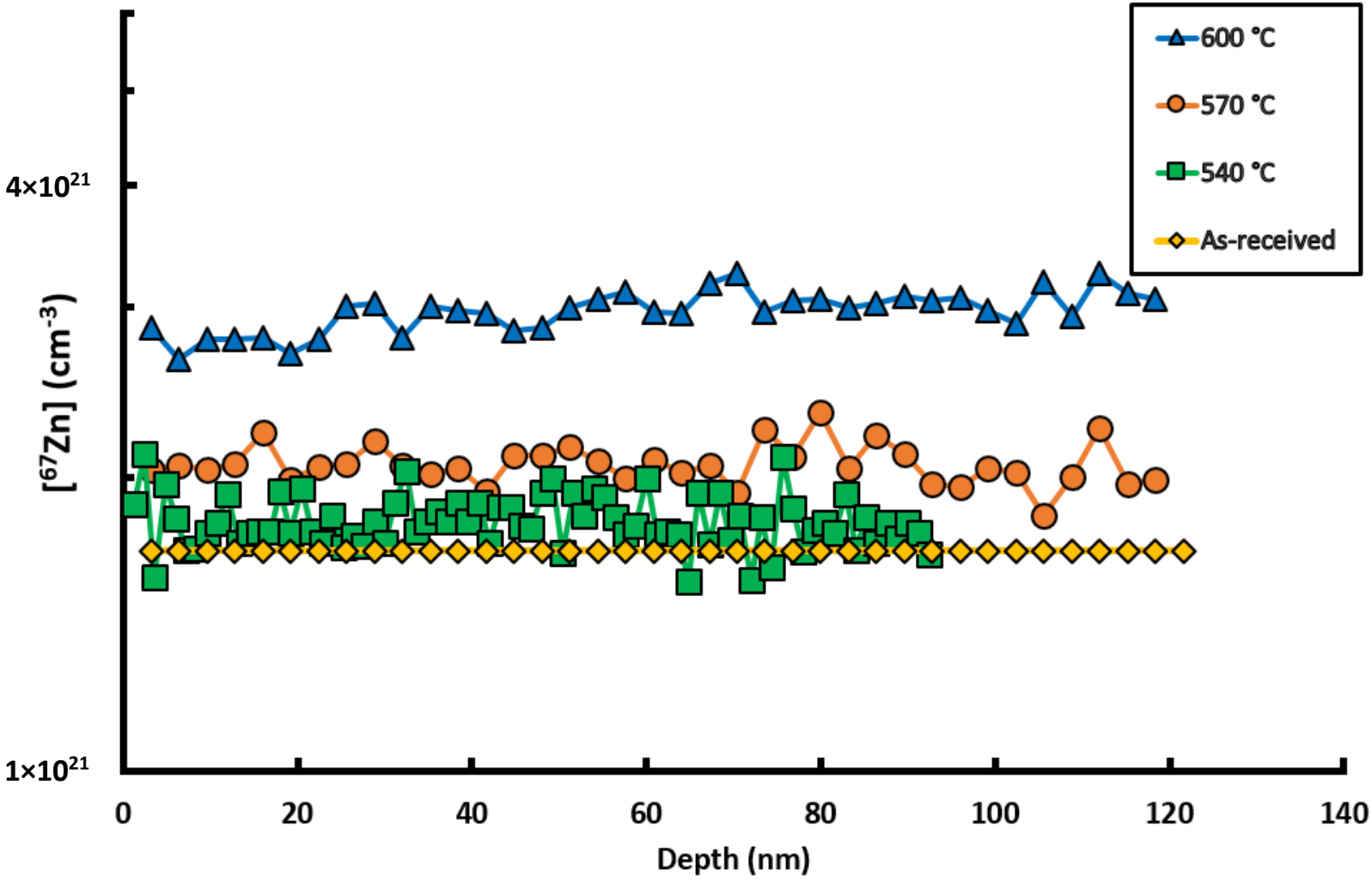

Figure 3.2 ^{67}Zn Diffusion Profile at oxygen pressure of 5×10^{-5} torr

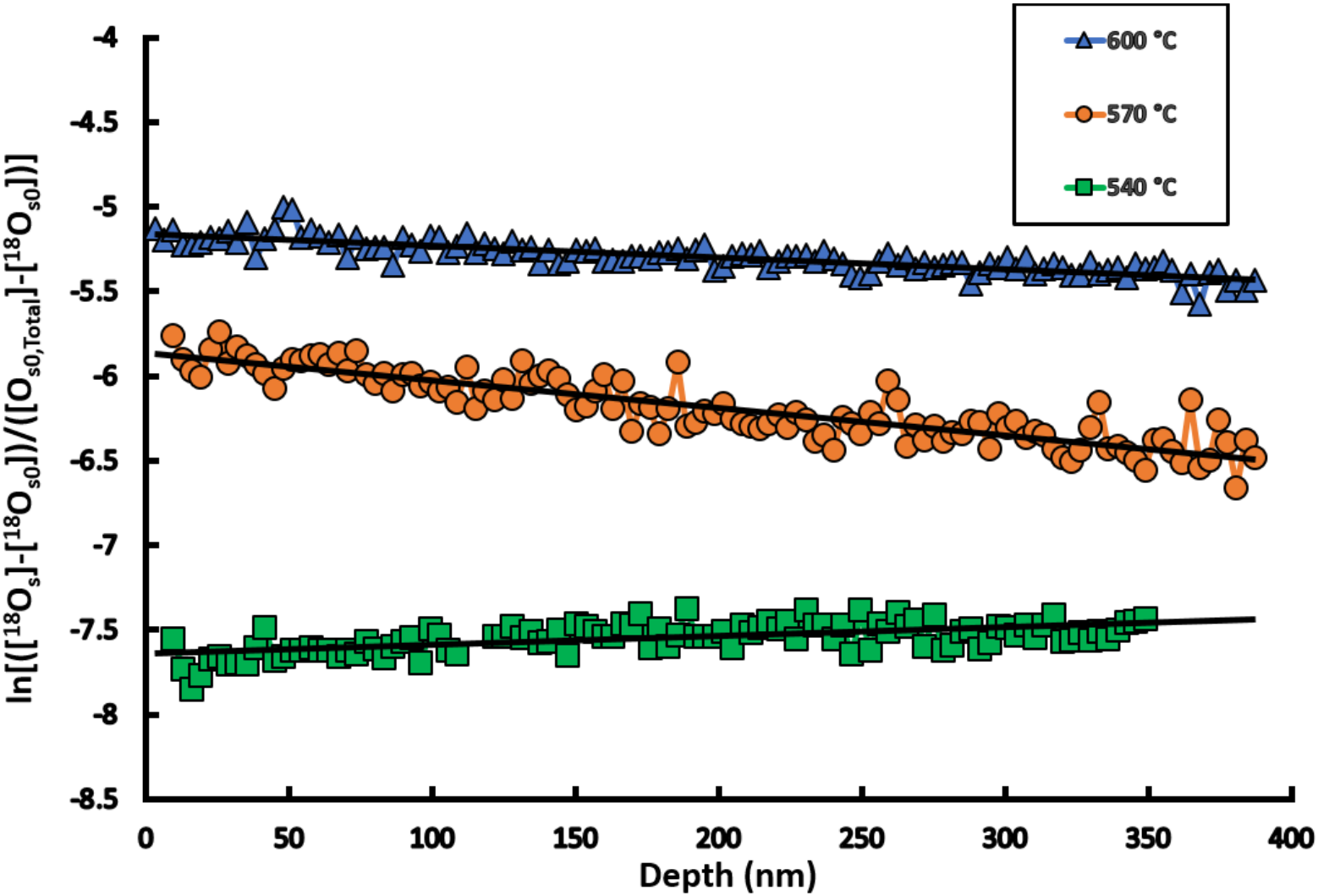

Figure 3.3 Kinetic factors extraction of ^{18}O diffusion profiles at different temperatures

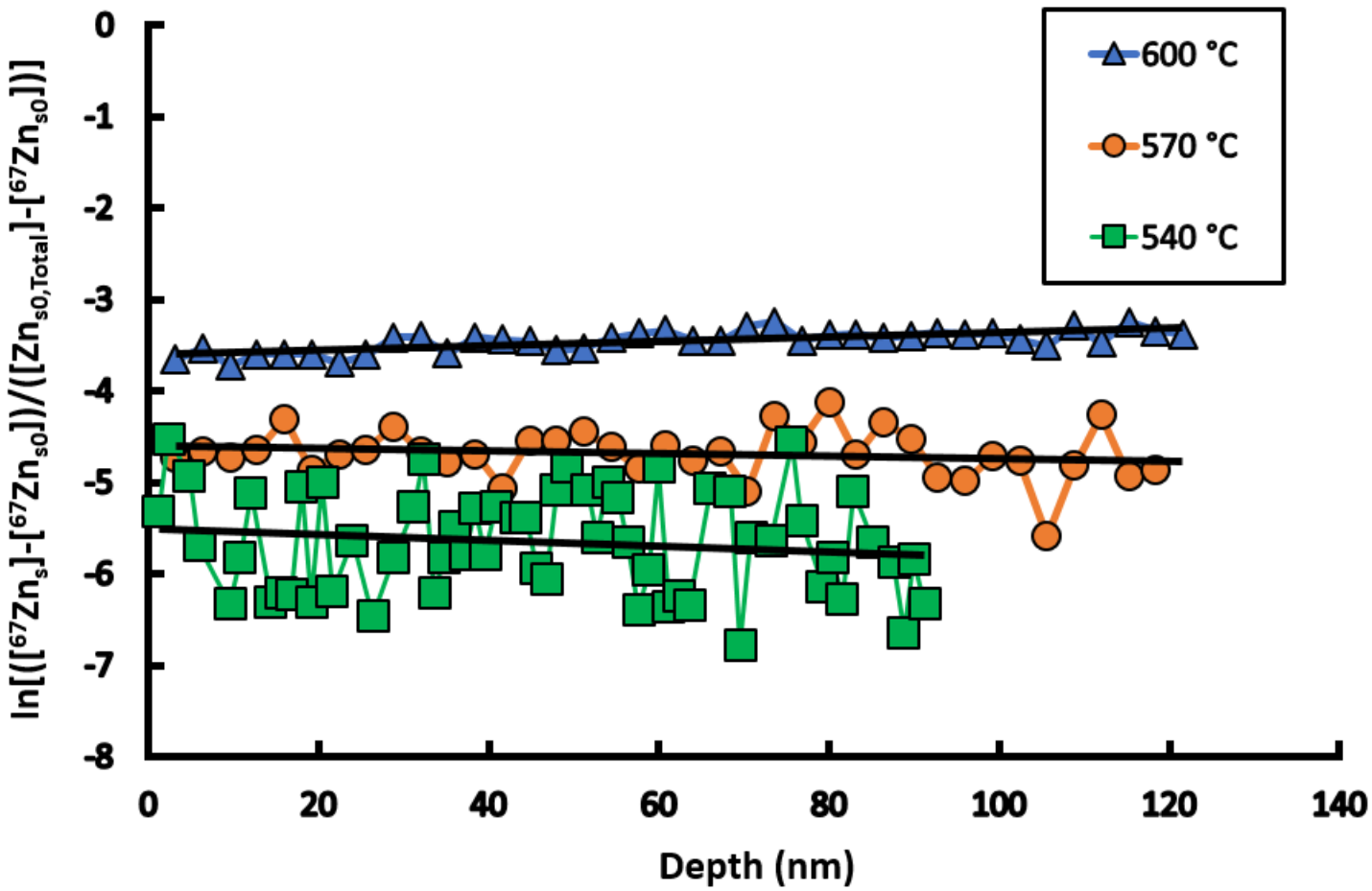

Figure 3.4 Kinetic factors extraction of ^{67}Zn diffusion profiles at different temperatures

	Temperature (°C)	λ (nm)	F ($cm^{-2}s^{-1}$)
^{18}O	600	1420	5.4×10^{12}
	570	625	1.17×10^{12}
	540	-2500	1.40×10^{12}
^{67}Zn	600	-417	3.92×10^{14}
	570	714	3.98×10^{13}
	540	332	8.52×10^{12}

Table 3.1 Kinetic Factors extract by analytical model

3.6 References

[1] E.G. Seebauer *et al.*, Mater. Sci. Eng. R-Rep. 70 (2010)

[2] A. G. Hollister *et al.*, Appl. Phys. Lett 102 (2013)

[3] M. Li *et al.*, J. Phys. Chem. C, 120 (2016)

[4] E. G. Seebauer *et al.*, Phys. Rev. Lett. 97 (2006)

[5] K. Gilliard, PhD Thesis, University of Illinois at Urbana-Champaign, 2017

[6] M. Li, PhD Thesis, University of Illinois at Urbana-Champaign, 2016

[7] P. Gorai *et al.*, Appl. Phys. Lett. 108 (2016) 241603

[8] P. Gorai *et al.*, Appl. Phys. Lett. 103 (2013) 141601

[9] P. Gorai *et al.*, ECS J. Solid. State. Sci. Technol. 1 (2012)

[10] E. Seebauer *et al.*, *Charged Semiconductor Defects*: *Structure, Thermodynamics and Diffusion* (2009)

[11] A. Janotti *et al.*, Phys. Rev. B 76 (2007) 165202

[12] P. Erhart *et al.*, Appl. Phys. Lett. 88 (2006) 201918

[13] G. Huang *et al.*, Solid State Commun. 149 (2009)

[14] L. S. Vlasenko *et al.*, Phys. Rev. B 72 (2005) 035203

[15] M. Li *et al.*, Appl. Surface Sci. 397 (2017)

[16] P. Gorai *et al.*, J. Appl. Phys. 111 (2012) 094510

Chapter 4: Room Temperature Photoluminescence of Annealed ZnO (0001) Single Crystals Under Different Oxygen and Zinc Environments

4.1 Introduction

Photoluminescence (PL) Spectroscopy is a powerful technique to measure the emission specific energy states within semiconductors. Those states mainly come from defects, and PL can be used as a direct measurement technique to analyze those defect states. As a large band gap material (3.37 eV) at room temperature, ZnO has received a lot of attention because of its strong luminescence properties and the potential for use in UV and green light emission devices [1-3]. The emission spectrum of ZnO contains two main parts: UV emission originating from excitonic emission near the band gap [4] and broad green emission (centered around 2.4 eV) that is related to the interband defect states [4-7]. In contrast to the near band gap excitonic emission, which is well understood, the mechanism of the visible emission is still in controversy. Various candidates such as oxygen vacancies (V_O^{2+}), zinc interstitials (Zn_i^{2+}), oxygen antisite (O_{Zn}), and even foreign atoms such as Cu are widely discussed, but none of them have explained all the published results [8]. In addition to single point defects, complex defects and defect clusters appear to affect the green emission [9].

Based upon research from this group, the atomically clean surface has been proven to open effective pathways for defect creation and annihilation. Due to the lower coordination number of the surface atoms requiring less bond creation and breakage for defect formation, the activation barriers for near surface pathways should be lower than those in the deep bulk [10-14]. Hence, the defect concentration for samples with clean surfaces should be more likely to reach equilibrium. Previous work from isotopic gas-solid exchange experiments in ZnO shows that a clean surface provides effective pathways for oxygen thermal injection into the bulk via a highly mobile species, the oxygen

interstitial (O_i), to annihilate oxygen vacancies (V_O) in the bulk. PL has been used as a supplementary technique to give quantitative evidence for the annihilation of V_O [10]. However, the results were analyzed based on an assumption that the origin of the broad green emission is only V_O. This assumption is probably not be true as the green emission peak is very wide (from 450 nm to 600 nm), and a single type of point defect is unlikely to yield such a broad peak. Instead the broad peak probably represents the composite of several different types of defects [7,15].

Among those defects could be those related to extrinsic hydrogen. Unintentional introduction of hydrogen is hard to avoid in almost all ZnO growth and processing environments [8,16,17]. First principles calculations show that hydrogen atoms can bond with and substitute for the lattice oxygen atoms to form stable and shallow donors in ZnO [16,18]. There are also some experimental results suggesting that trapped hydrogen molecules can dissociate into H_i and H_O and, and that they will not totally dissociate until 700 °C [19,20]. Although there is good evidence that hydrogen is widely existent in ZnO, PL emission resulting directly from to hydrogen-related defects has not been much discussed in the literature.

In this chapter, the annealing oxygen pressure and temperature dependence of ZnO PL spectra in the presence of both oxygen and zinc injection will be discussed. It is found that both O_i and hydrogen are likely involved in 503 nm and 547 nm green emission, probably forming emissive complexes. The main effect of Zn_i is indirect, by slowing down O_i diffusion (perhaps through complexes). It is also a likely that H_2 trapped in ZnO during processing plays an essential role in yellow-red emission.

4.2 Experiment

The sample preparation procedures were detailed in the previous chapter.

The PL experiments were mainly conducted in a custom-built room temperature photoluminescence (RTPL) instrument in the Frederick Seitz Materials Research Laboratory, and part of the time in a resolved photoluminescence (TRPL) setup in the MRL laser lab. The general setup of the PL can be obtained from the laser lab and will not be discussed here.

For RTPL, the ZnO (0001) Zn-terminated face specimen (in dimension of 1 cm × 0.5 cm × 0.05 cm) was held by vacuum backed vertical sample mounts. The sample preparation procedures were detailed described in chapter 2. To mitigate luminescence from other sources (e.g., the sample mount), the specimen should be put on the center of the sample mount, where the laser may be aligned to the hole on it to mitigate background noise. The sample was excited by a 266 nm Q-switched Nd:YAG laser with power of 0.1 mW. Since the 266 nm laser barely penetrated the neutral density filter, the incident laser power was controlled and calibrated by a linear polarizer. The beam alignment was extremely important for this experiment, as a slight twist of the mirror in the setup could cause significant differences in the magnitude of intensity of PL spectrum. However, due to the setup being located in a shared-use facility, it's better to map and record the setup for an experiment in case of anyone changed it.

The UV laser beam diverged a lot on the path to the sample, the power of the beam that emerged from the polarizer might not be proportional to beam power on the sample. To increase the accuracy and reproducibility, the laser power was measured by a power meter which was put about 3 cm away from the top of the sample. PL spectrum for controlled sample should be measured every time before the experiment to check the performance and alignment of the PL setup. To collect the

data, depending on the magnitude of PL intensity needed, the exposure time for the CCD camera could be varied. Here 5 seconds exposure time was chosen. Further analysis, which included the Gaussian peak fitting, of the PL spectra was done by the software package OriginPro 2017 by picking the peak centers at 503 nm (FWHM around 76 nm), 547 nm (FWHM around 107 nm), 603 nm (FWHM around 91 nm), 650 nm (FWHM around 13 nm), and 676 nm (FWHM around 32 nm).

4.3 Results

Figures 4.1, Figure 4.2, and Figure 4.3 show the PL spectra of samples processed under different conditions. These spectra all show an asymmetric broad emission peak in the green range. Compared with the as-received sample, regardless of exposure to zinc or not, all specimens showed some blue shift of the broad green emission peak. As discussed below, the broad green band is Gaussian divided into three components, 503 nm, 547nm, and 603 nm emissions, which are proposed to be due to the transitions related to defects in ZnO. The fitted spectra are shown in Figure 4.14.

From Figure 4.4, 4.5, we can clearly see that the at same annealing pressure I_{503nm} and I_{547nm} (here I_{503nm} and I_{547nm} represent the height of 503nm and 547nm Gaussian fit peaks respectively) show positive correlation to the annealing temperature, and simultaneous exposure of zinc flux doesn't change this trend but decrease the emission height. For samples annealed above 1×10^{-5} torr oxygen background pressure, simultaneously annealing with zinc flux will result in decreased value of I_{503nm} and I_{547nm}. On the other hand, for samples annealed at 1×10^{-5} torr oxygen background pressure, exposure of zinc flux gives us totally different result, which has greater I_{503nm} and I_{547nm}. Beside suppressing I_{503nm} and I_{547nm} a bit, introduction does not significantly affect the temperature dependence for I_{503nm} and I_{547nm} too much.

Figure 4.9, 4.10 show the pressure dependence of I_{503nm} and I_{547nm} at different annealing temperature and ambient. For samples annealed under an oxygen-only environment, I_{503nm} and I_{547nm} show an overall positive correlation respect to annealing pressure. For samples injected with zinc, above 540 ˚C, both I_{503nm} and I_{547nm} show an overall positive annealing pressure dependence, but at 540 ˚C it displayed an inversed relation. Overall, the pressure dependence for I_{503nm} and I_{547nm} looks like the mirror image of each other.

The temperature dependence for I_{603nm}, I_{650nm}, and I_{675nm} (Figure 4.6-4.8) are like each other but quite different respect to I_{503nm} and I_{547nm}. In a pure oxygen environment, the temperature dependences of I_{603nm}, I_{650nm}, and I_{675nm} are very small below 1×10^{-4} torr. At 1×10^{-4} torr oxygen pressure, the temperature dependences for I_{603nm}, I_{650nm}, and I_{675nm} are nonmonotonic, where I_{603nm}, I_{650nm}, and I_{675nm} increase from 540 ˚C to 570 ˚C, but decrease from 570 ˚C to 600 ˚C. Exposure to zinc flux mute this relationship a bit, but overall similar to the samples expose to oxygen only.

Figure 4.11, 4.12, and 4.13 show the pressure dependences for I_{603nm}, I_{650nm}, and I_{675nm}. At the same annealing temperature, the pressure dependence for those three peaks are largely like each other, and exposure to zinc flux don't affect the trend too much but suppress the emission a little bit. Overall, I_{603nm}, I_{650nm}, and I_{675nm} increase with increased annealing pressure, but the relation is not monotonic, and the lowest emission occurs at 5×10^{-5} torr.

4.4 Discussion

4.4.1 Background of PL emission in ZnO

ZnO often exhibits very broad green to red luminescence, with a composite peak typically centered between 500 and 600 nm [8, 57,58]. In the literature, the broad emission is predominantly assigned to V_O, V_{Zn}, and sometimes O_{Zn} [8,57,58]. Different experimental techniques suggest different possibilities for the defect identities.

A lot of literature assigns the 490-540 nm component peak (roughly 2.29-2.53 eV) to V_O, based on an EPR peak at g~1.96 [6,21,22], suppression of the 2.29-2.53 eV emission with annealing under an oxygen environment [4,23,24,25], and increased 2.37 eV emission after annealing vacuum and N_2/H_2 annealing [21]. However, those results contradict other observations that green emission centered at 2.28 eV increases after oxygen annealing [26,27], and green emission declines after electron irradiation of a ZnO single crystal, which produces excess V_O in the bulk [28,29].

Other than V_O, V_{Zn} is also sometimes assigned as a possible contributor for green emission. Some experimental results involving hydrogen annealing show that hydrogen attenuates the emission center around 520 nm (2.4 eV) and the EPR signal at g~2.034 [8,30], which are believed come from V_{Zn} [31,32]. However, opposite behavior is reported by others [33,34,35], wherein the green emission becomes broader and larger after hydrogen annealing. Other reports also suggest a possibility that V_{Zn} can lead to a red emission center around 680 nm by coupling with other donors and acceptors [28,29,36].

The conflicting hypotheses regarding the origin of green emission and its components may partly reflect the importance of nearby surfaces in influencing the diffusion-reaction network of defect in the bulk. Atomically clean surfaces have been proved to open effective pathways for defect

creation and annihilation, which result in more rapid approach of native defect concentrations to equilibrium [10-14]. A large fraction of the experiments were conducted using ZnO nanoparticles of various shapes [27,33,37,38,40] and ZnO polycrystalline powder [30] and thin film [39] under non-high-vacuum environments, in which case the surface conditions were not well controlled and were unlikely to be sufficiently clean for efficient O_i injection. The high surface/volume ratio and grain concentrations in the specimens may amplify the influence of non-clean surface. Limited experiments have been done with bulk single crystal ZnO [22,25,28,36,41]. Those experiments employed several treatment protocols, including thermal annealing in various gases and nonthermal methods such as plasma treatment and electron irradiation. These reports also have led to conflicting results. For example, Refs. [22] and [28] claim green emission comes from V_O, Ref. [25] suggest green emission relate to both V_O and V_{Zn}, Refs. [41] claim green emission come from V_O related complex, but Ref. [36] claim the green does not relate to V_O but rather the acceptor introduced during the electron irradiation.

Beside the influence of a clean surface, the inconsistent hypotheses raise the possibility that the green emission may originate, not only from native point defects, but also from complexes of native defects [42, 43] with each other or with unintentional extrinsic impurities [44,45,46]. If such impurities exchange readily with the gas phase, sample processing history may play a significant role in the PL emission.

One especially important unintentional extrinsic defect in ZnO is hydrogen. Common ZnO growth techniques like the gas-transport [17] and hydrothermal methods [16] can't eliminate the hydrogen contamination even in principle. Similarly, ZnO nanoparticles, which are widely used in defect studies [47-50], involve growth under the environments rich in OH^-. The literature attributes the emission behavior change after hydrogenation in ZnO to indirect effects: passivation of deep

donor and acceptor defect states [38,40,41,51,52], passivation of non-emissive centers [53], and creation of V_O due to the loss of oxygen [33]. However, hydrogen has not been discussed as a factor that directly causes green emission, and the non-well-controlled protocols with respect to hydrogen in different literature reports may result significant differences in the luminescence behaviors.

4.4.2 Defects contributing to green emission

We can see that after annealing, all 5 fitted emission peaks show significant enhancement compared to the as-received sample. It's extremely unlikely for a single type of defect like O_i to be responsible for the emission over such a broad wavelength range. We believe that the overall enhancement of PL spectra is caused by annihilation of V_O. The yellowish as-received sample contains a substantial amount of V_O (known due to the slightly yellow color) and the dominant V_O, whose energy level is located around ½ E_g above the VBM [72], is likely to be very effective in reducing the lifetime of the minority photogenerated carriers. In this physical picture, the non-radiative recombination induced by V_O decreases the likelihood that the minority carriers participate in emissive transitions, which results in reduced PL emission. The annihilation of V_O would decrease such an effect and increase the PL emission throughout the wavelength range.

From Figure 4.4, 4.5, we can clearly see that both I_{503nm} and I_{547nm} increase with increasing annealing temperature and oxygen pressure, their temperature and pressure dependences are large like each other. This observation suggests that the defects that contribute to I_{503nm} and I_{547nm} both involve O_i in some way. This result agrees with the SIMS observations, which show the net flux of O_i dramatically increases with temperature and oxygen pressure for samples annealed in oxygen only environments [10]. In addition, for samples annealed under a 5×10^{-5} torr oxygen environment (Figure

4.4, 4.5), all samples show a trend that the both I_{503nm} and I_{547nm} decrease with exposure to Zn flux. This observation agrees with the SIMS results (Figure 3.1, 3.2) that at this pressure, the injection of Zn_i can inhibit the injection of O_i. However, it has been proved that the concentration of O_i in ZnO shows strong and monotonic positive relation to the annealing temperature and oxygen pressure [54]. From our PL spectra, we can't see such a strong and consistent I_{503nm} and I_{547nm} dependence with respect to temperature. This behavior suggests that the emission center at 503 and 547 nm comes from a combination of O_i and a non-well-controlled impurity affected by sample processing history.

One possible impurity of this kind is hydrogen. Hydrogen is known to exist in at least three forms within ZnO [8,19,20,55], a body-centered interstitial H_i inserted between Zn and O atoms [16], a substitutional H_O form at an oxygen site [55], and in molecular form as H_2 that is typically trapped [19,20]. These species and concentrations can interchange with each other in a complicated way and do not show monotonic concentrations with respect to temperature [19]. Proximity to a surface, annealing time, and other aspects of the sample processing history can play a major role [19,20]. It has been reported that hydrogen annealing can induce dramatically different emission behavior in ZnO treated by different methods [35,51]. Hence, it's reasonable to believe that oxygen pressure can also play similar role if oxygen (especially as O_i) couples to hydrogen species that reside in ZnO.

4.4.3. Effects of Zn_i on green emission

Many studies conclude that Zn_i is a shallow donor which are located around 0.1 – 0.22 eV below the CBM [8, 56,57], so Zn_i itself can't contribute to the green emission. SIMS profile (Figure 3.2) shown in the last chapter give strong evidence that vast amount of Zn_i diffuse into the bulk structure.

It therefore seems likely that Zn_i and/or O_i can incorporate into a relatively stable intermediate or defect complex, which indirectly affects the concentration of the defects that contribute directly to the emission.

From Figure 4.9, 4.10, we can observe that with zinc flux, I_{503nm} and I_{547nm} decrease with increased annealing oxygen pressure at low temperature. This trend gradually reverses with increased annealing temperature until upon reaching 600 °C, both I_{503nm} and I_{547nm} show overall positive pressure dependence. On the other hand, without exposure to zinc flux, I_{503nm} and I_{547nm} show a general positive pressure dependence regardless the temperature. As both 503 nm and 547 nm emission most likely have some relation to O_i, the negative oxygen pressure dependence of I_{547nm} should not be expected for our clean surface injection model, unless O_i form some stable non-radiative centers in the bulk during the diffusion. For example, $O_2 \overset{K_1}{\Leftrightarrow} [Intermediate] \overset{K_2}{\Leftrightarrow} O_i$. When the temperature is low, more O_i prefer to aggregate into the intermediate, but at high temperature they are easier to release into the deep bulk. This agrees with the SIMS results (Table 3.1) that diffusion length for O_i is cut by injection of zinc. In this case, the introduction of Zn_i seems to play an essential role in the concentration of intermediate.

It shows some similarities to the extended defect behaviors that are well studied in boron implanted silicon [58] in which case the extended defects work as stable intermediates that both absorb and release point defects. This type of extended defect has also been well studied in oxygen injected rutile TiO_2, where extended defects work as an intermediate to sink and release Ti_i and O_i into bulk TiO_2 [59]. In ZnO, there is no evidence for large interstitial clusters, but smaller complexes of O and Zn may be found. Actually, there is evidence showing that Zn_i is highly mobile at low temperature, and it likely to form a stable complex [60-63]. The vibrational mode at 509.5 cm^{-1} also

concluded as Zn_i-O_i by Raman spectroscopy [64,65]. However, with the complicated behavior, further study in broader annealing temperature and pressure range may help us to understand this system.

4.4.4 Defects contributing to orange-red emission

The gaussian fitted spectra can be divided into two major parts: 1) green emission consisting of the 503 and 547 nm peaks, which show similar dependence upon annealing pressure and temperature, and 2) orange-red emission involving the 603, 650, and 675 nm peaks, which show similar annealing pressure and temperature dependence to each other, but clearly differ from the responses of green emission.

In ZnO, studies of orange-red emission are much less common than for green emission and typically involve annealing in oxygen. The literature reports orange-red emission centered in the general region between 580 and 700 nm. The constituent peaks are generally much broader and higher than our results [36,39,66,67,68], and typically overlap or passivate the green emission part. One famous hypothesis is that red emission centered at 680 nm comes from V_{Zn} and a V_{Zn}-related complex [28,29,36]. It has been reported that electron irradiation treatment, which creates many vacancy related defects, leads to a dramatic increase in the 680-nm peak [28,29,36]. Annealing the ZnO (without electron irradiation treatment) under an oxygen environment leads to similar enhancements in 680 nm emission, accompanied by increased 510 nm green emission [36]. On the other hand, annealing under zinc vapor can slightly attenuate the green and dramatically mute the red emission [36].

Although the temperature and pressure dependence of I_{603nm}, I_{650nm}, and I_{675nm} look like each other, there is no clear trend among them. The nonmonotonic behaviors of I_{603nm}, I_{650nm}, and

I_{675nm} respect to annealing oxygen pressure and temperature call to mind the behavior of hydrogen in ZnO. It has been reported that the body centered H_i can be trapped in ZnO by forming molecular H_2 [20, 69], which can't be totally annealed out below 700 °C [20]. The trapped H_2 shows similar 4150 cm^{-1} vibrational modes in Raman spectroscopy to gas phase H_2, which suggests that trapped molecular H_2 in ZnO may have similar properties in other ways to gas phase H_2 [20]. Furthermore, the 603 nm peak from our PL spectra are reminiscent of the well-known H_2 Fulcher band that is centered around 600 nm. The similar emission wavelength may indicate there are a connection among them. As hydrogen is hard to eliminate during a typical ZnO processing history below 700°C [19,20]. As our experiments were conducted below 600 °C, we probably have some molecular H_2 in our samples. Hence, we postulate that the 603 nm comes from the trapped H_2.

O_i is often assigned to the orange-red (580-670 nm) luminescence in ZnO [27,33,39,70]. The assignment of O_i has been supported by reduction of red emission after annealing under an oxygen environment [27]. Generally, the emission is often conceived as the transition from the conduction band minimum to O_i [27, 33,70] or from a state involving Zn_i near the CBM to O_i [39]. Although the other experiments give evidence that O_i can contribute to yellow-orange emission, in our system, we can exclude this possibility. Below is our reasoning. From the Figure 4.14 a), we can see that the as-received sample shows a persistent 650 nm emission peak. A revious group member has reported that the hopping barrier for O_i in ZnO can as low as 0.61 eV [7,']. The yellowish as-received sample has been reported has dominant amount of V_O [10,54]. It is very unlikely to have significant amounts of free O_i, especially when it has such low diffusion barrier so that the O_i can find sequestration sites upon quenching the annealing temperature. Hence, in our system, lone O_i should not be considered as the source of 650 nm emission like the other reports [33,39].

By literature review, it's not unreasonable to ascribe V_{Zn} as the source for 675 nm emission [28,29,36]. However, that assignment is not likely in our system. Our SIMS data (Figure 3.2) show solid evidence that large amounts of Zn_i have been injected into the bulk. The fast moving Zn_i [8] can annihilate the V_{Zn} which leave the treated sample V_{Zn} free. If the 675 nm emission comes from V_{Zn}, we may expect to see the I_{503nm} show negative temperature dependence. However, our PL spectra show the opposite relationship. Thus, V_{Zn} can't be assigned as the origin for the red emission at 675 nm.

Then it raises a question about the source of 650 and 675 nm emission. As the temperature and pressure dependence of I_{603nm}, I_{650nm}, and I_{675nm} look like each other in all their complicated details, it reasonable to postulate that the same type of defect induces 603, 650 and 675 nm emission. As the 603 nm emission most likely originates from trapped molecular H_2, the persistence 650 and 675 nm emission may likely relate to H_2 too. This hypothesis presupposes that the ZnO matrix changes the Fulcher emission band enough to give rise to 650 and 675 peaks that are beyond the range of Fulcher emission in the gas phase. That possibility is plausible, but there is presently no further independent evidence for it. Further study is needed.

4.5 Conclusion

Simultaneous zinc and oxygen thermal injection through the Zn-terminated ZnO (0001) clean surface has been studied via photoluminescence. The spectra are gaussian fitted by 5 peaks centered at 503, 547, 603, 650, and 675 nm. It was found that the injection of O_i results in increased 503 and 547 nm peaks, and introduction of Zn_i passivates the emission a bit above 1×10^{-5} torr oxygen annealing pressure but does not change their temperature and pressure dependence significantly.

However, the temperature and pressure dependence for I_{503nm} and I_{547nm} are not monotonic. We believe that the 503 and 547 nm peaks come from defects related to both O_i and hydrogen, with important possibilities being the complexes O_i-H_i and O_i-H_O. The modest effects of gaseous Zn on the PL, together with the SIMS results of Chapter 3, suggest that Zn_i influences the PL through the inhibition of O_i injection and diffusion by forming non-emissive intermediates. In addition, we surmise the 603, 650 and 675 nm peaks originate from H_2 molecules trapped in ZnO, with the rationale being the spectroscopic similarity of the 603 nm peak to the gas-phase H_2 Fulcher band and the similar complicated behavior of all three peaks in response to the treatments of O_2 and O_2 + Zn. O_i and V_{Zn} are not likely contribute to the 650 and 675 nm peaks.

4.6 Figures

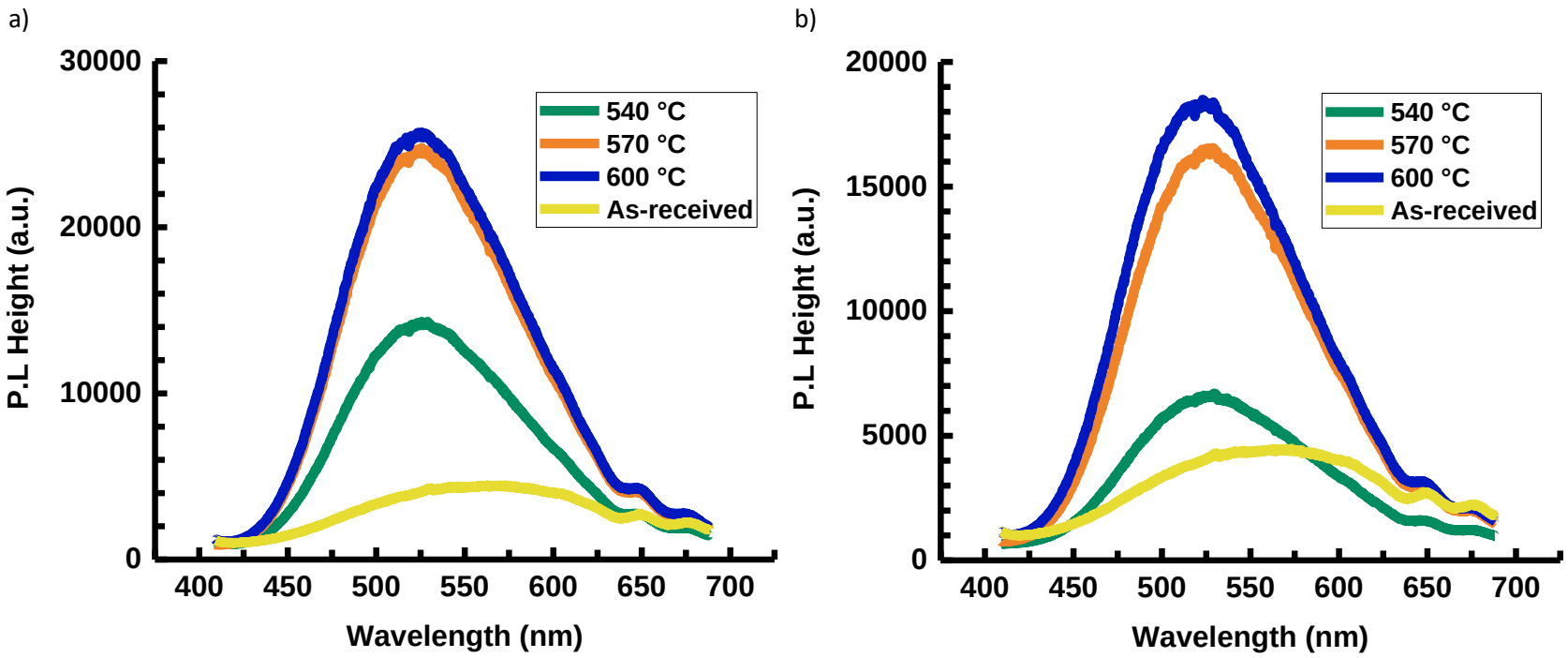

Figure 4.1 PL spectrum for samples annealed in 5×10^{-5} torr a) pure oxygen b) with zinc flux

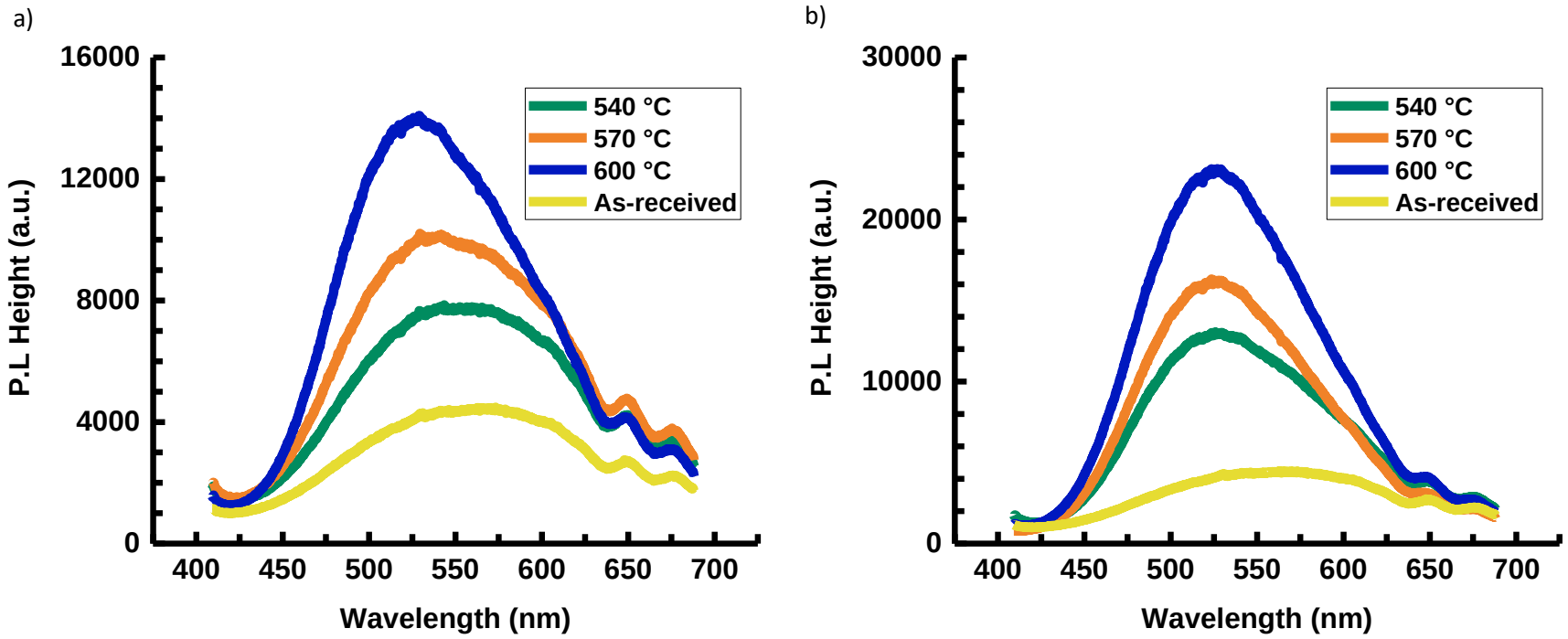

Figure 4.2 PL spectrum for samples annealed in 1×10^{-5} torr a) pure oxygen b) with zinc flux

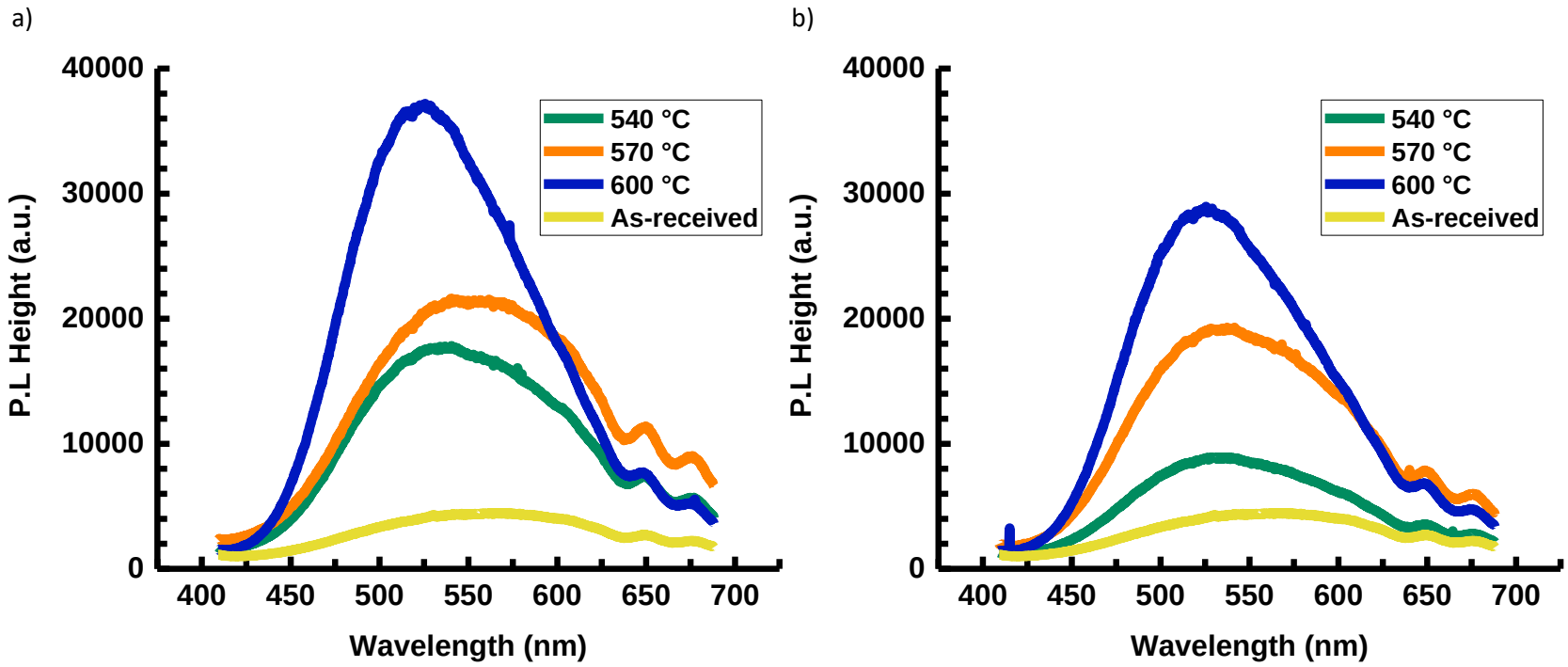

Figure 4.3 PL spectra for samples annealed in 1×10^{-4} torr a) pure oxygen b) with zinc flux

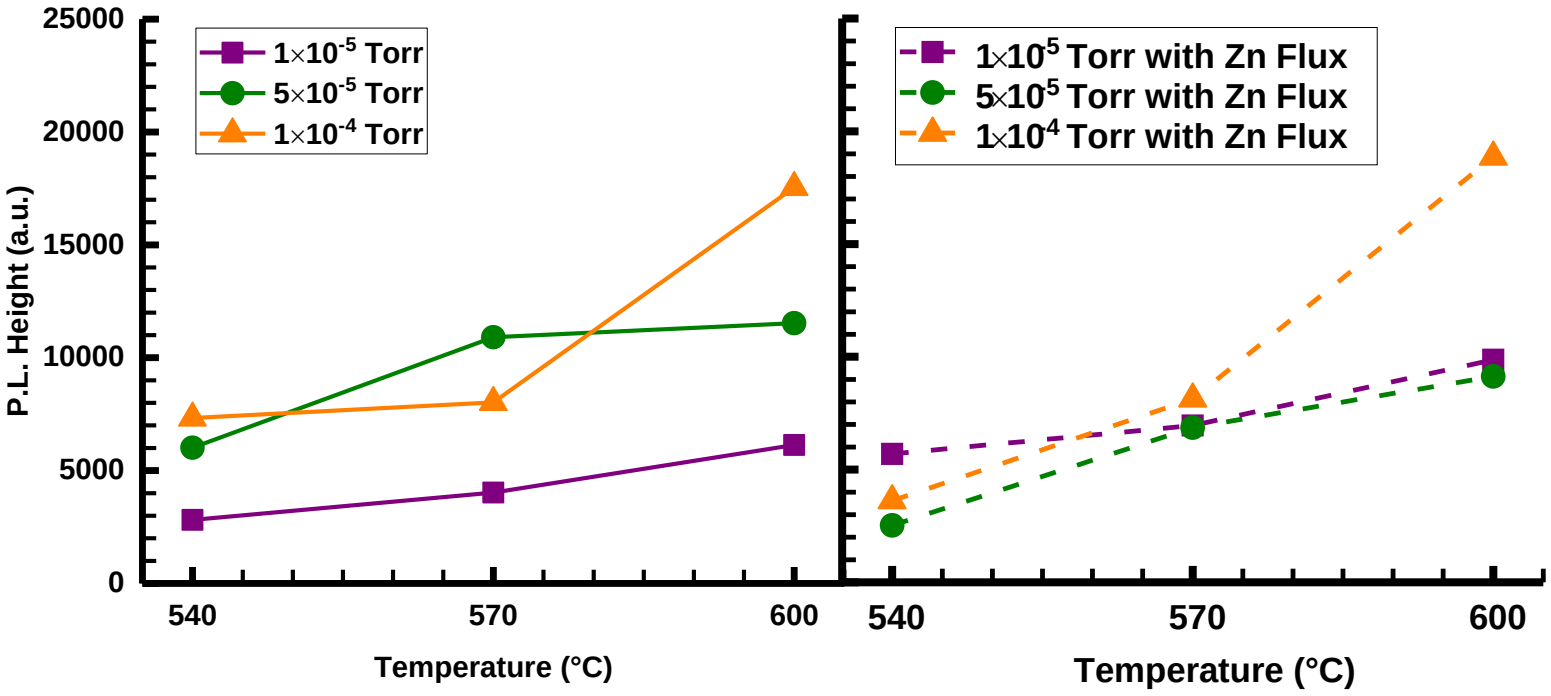

Figure 4.4 Temperature dependence for 503 nm peak

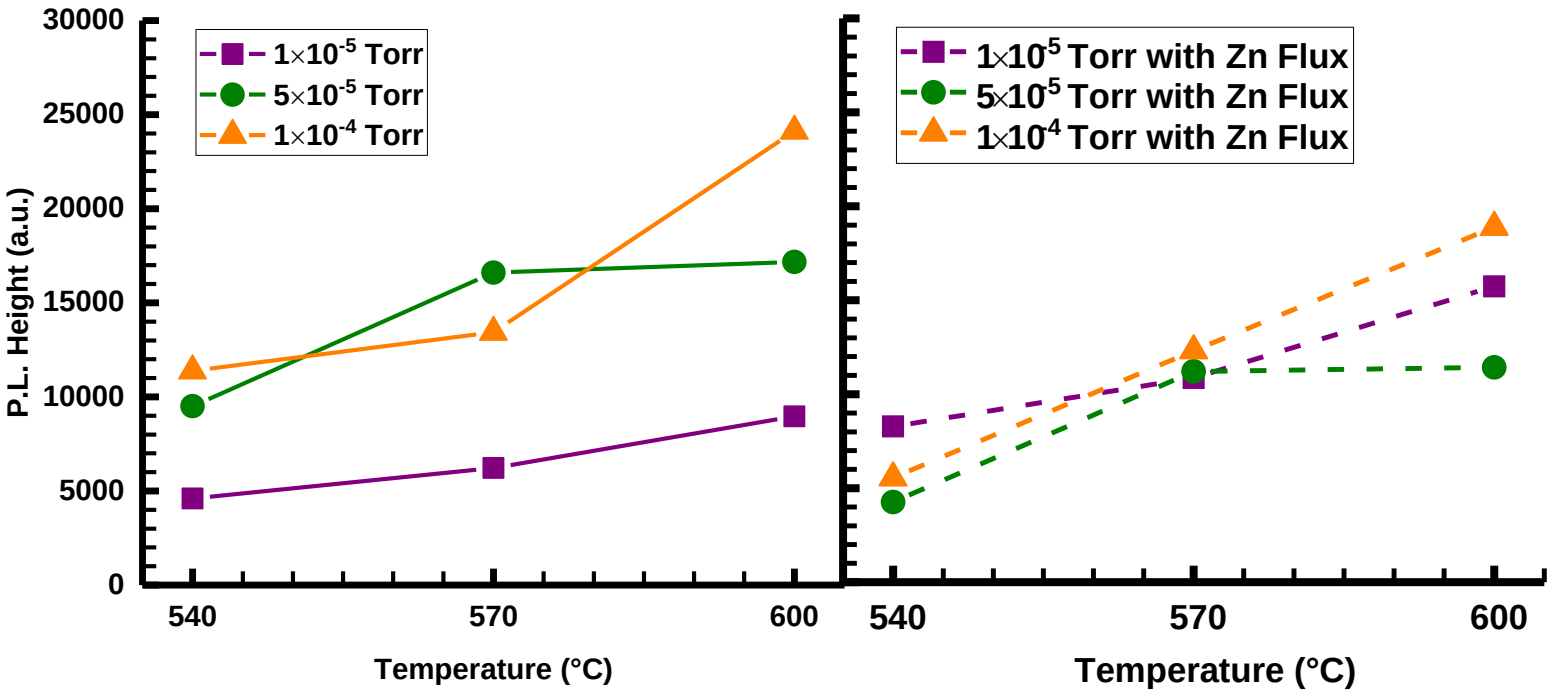

Figure 4.5 Temperature dependence for 547 nm peak

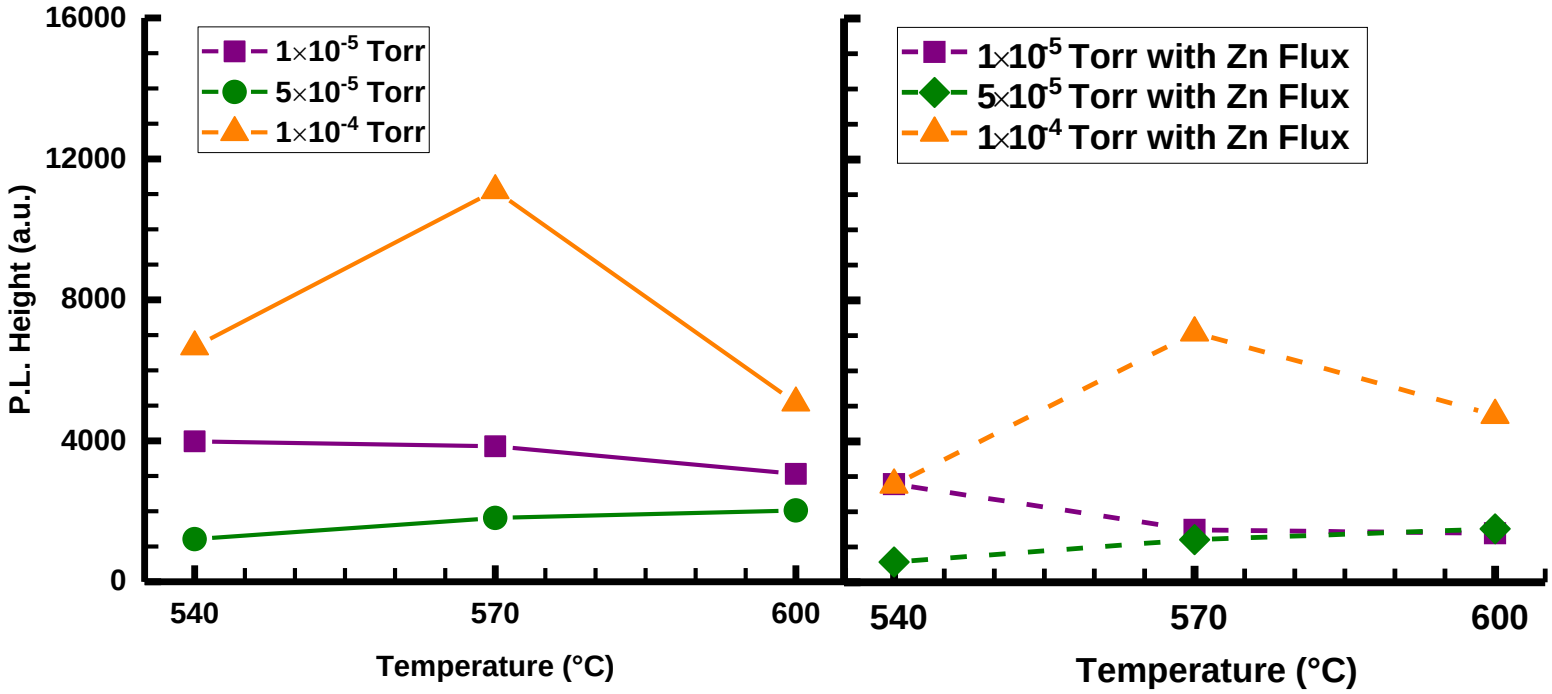

Figure 4.6 Temperature dependence for 603 nm peak

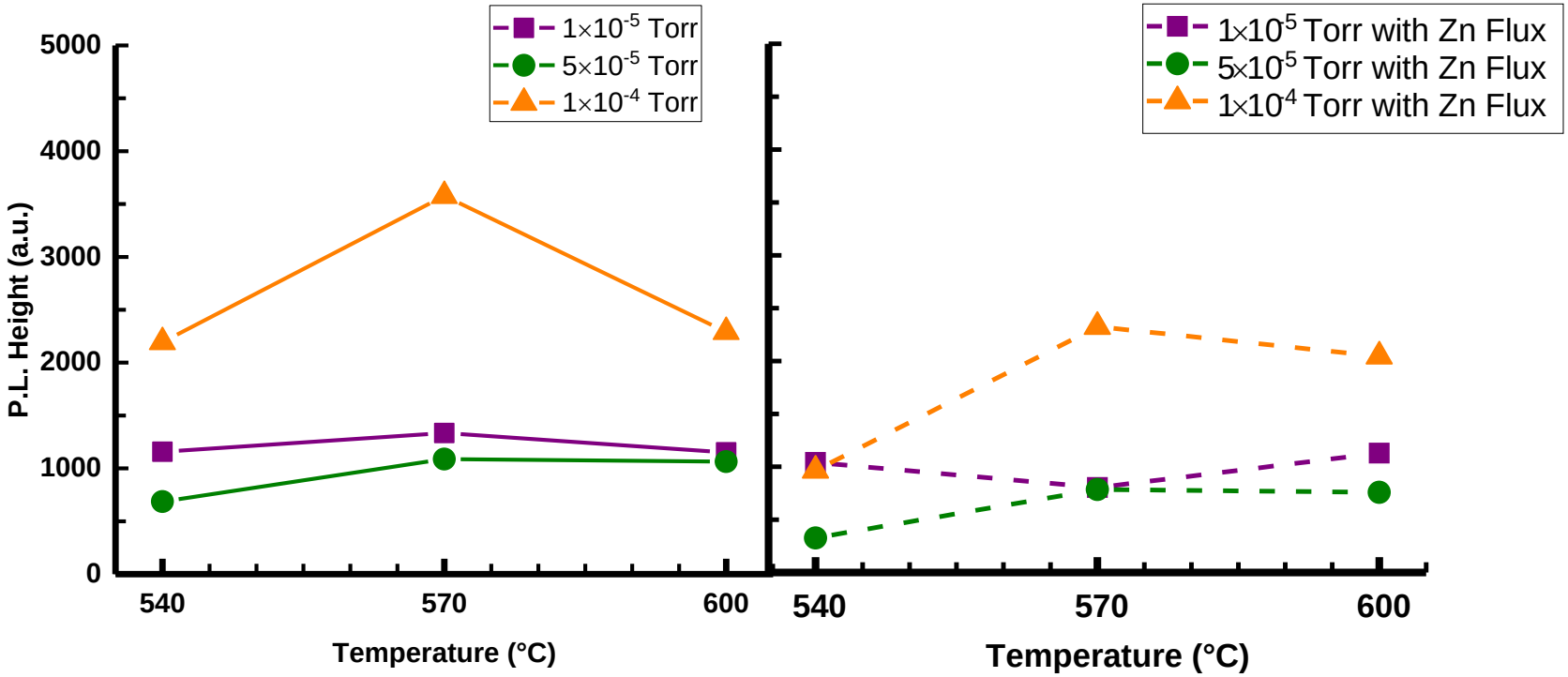

Figure 4.7 Temperature dependence for 650 nm peak

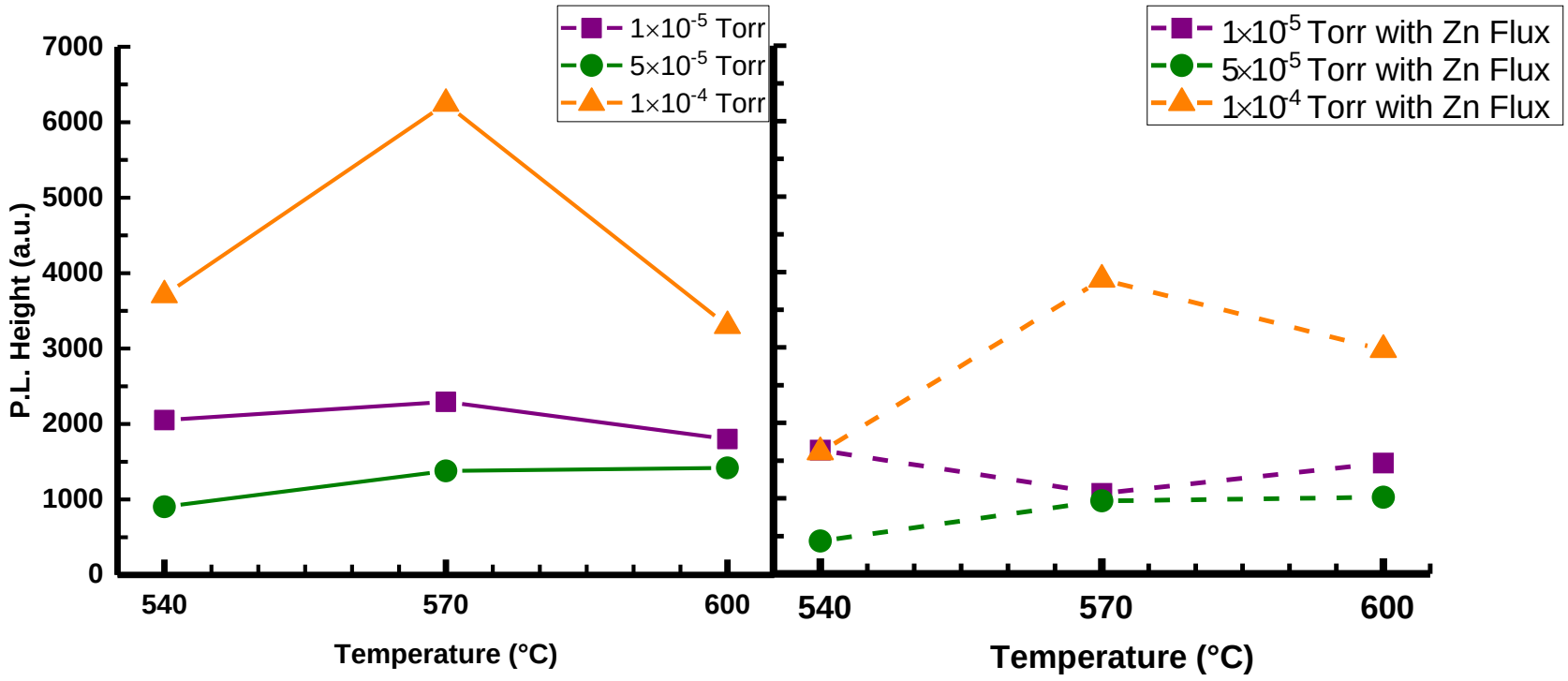

Figure 4.8 Temperature dependence for 675 nm peak

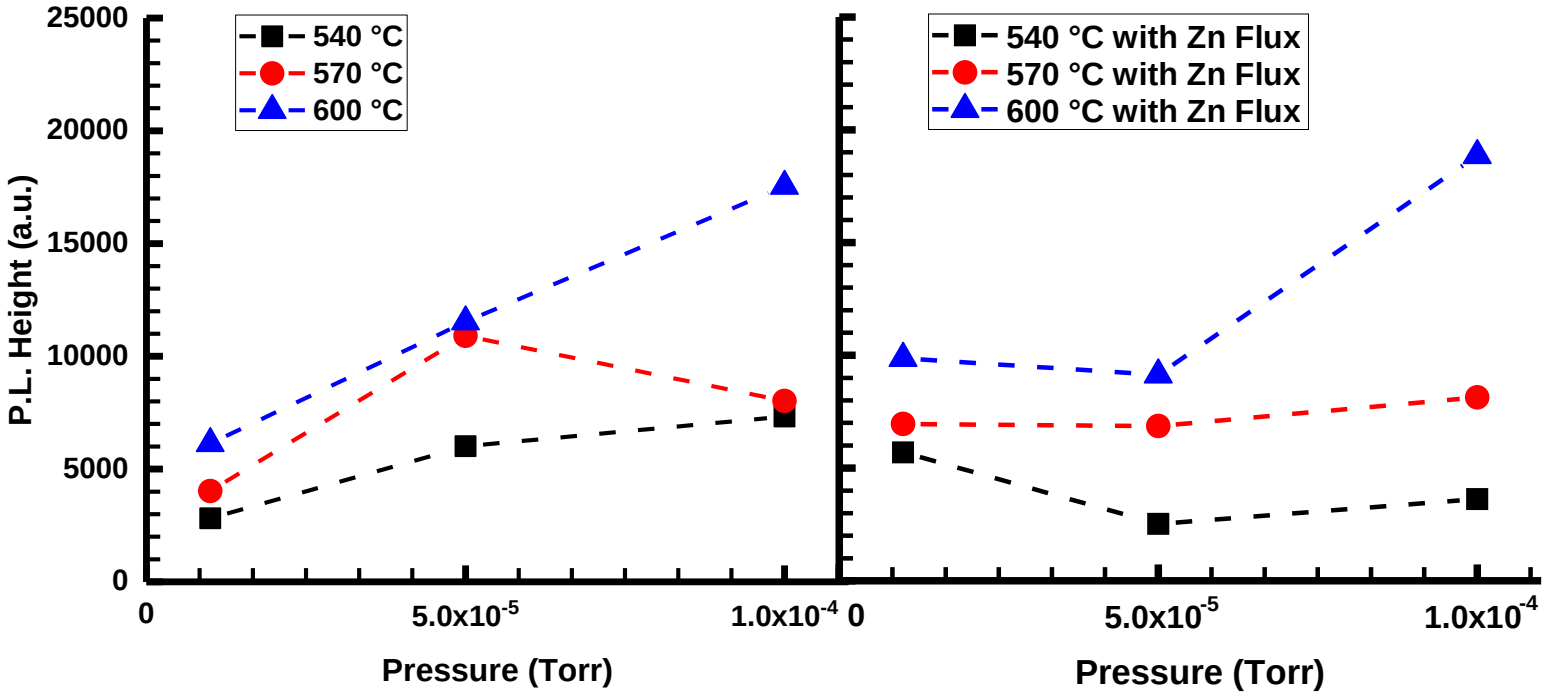

Figure 4.9 Pressure dependence for 503nm peak

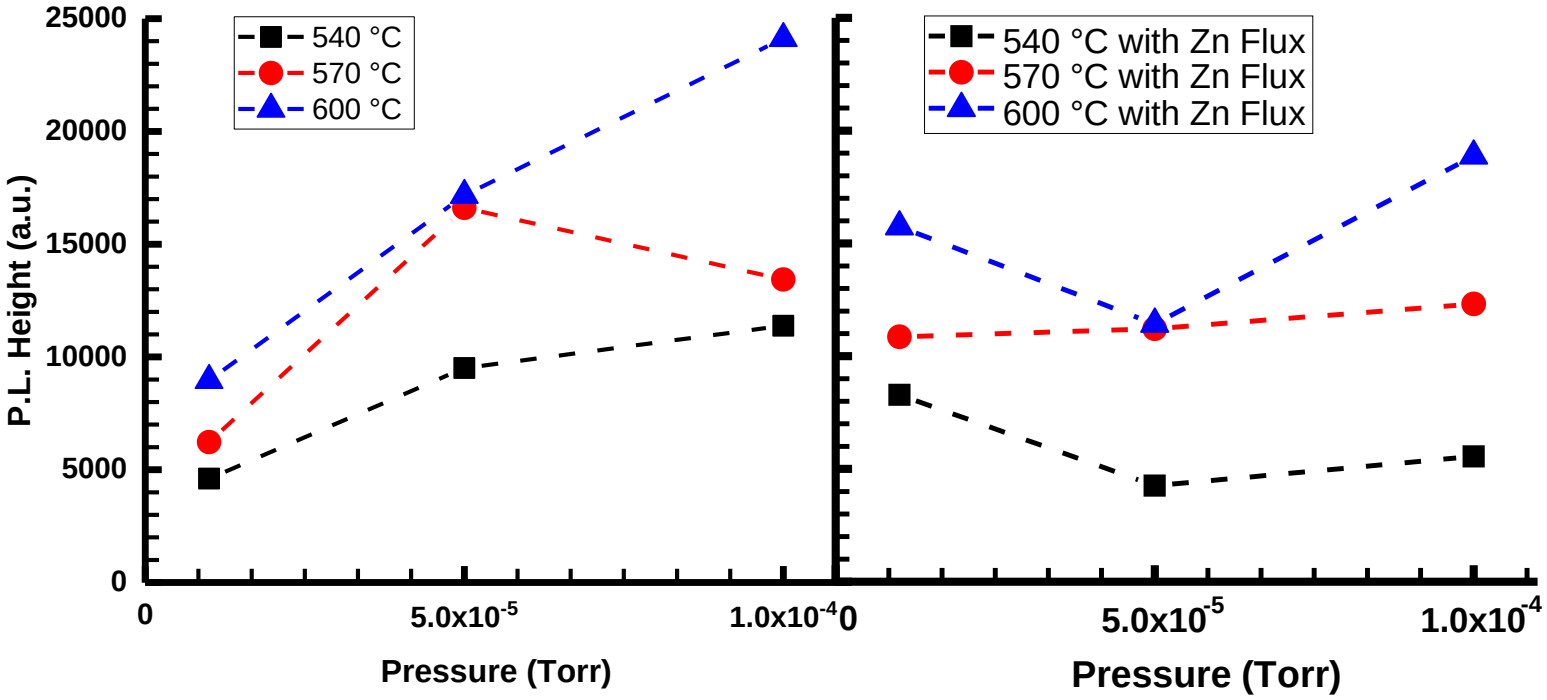

Figure 4.10 Pressure dependence for 547 nm peak

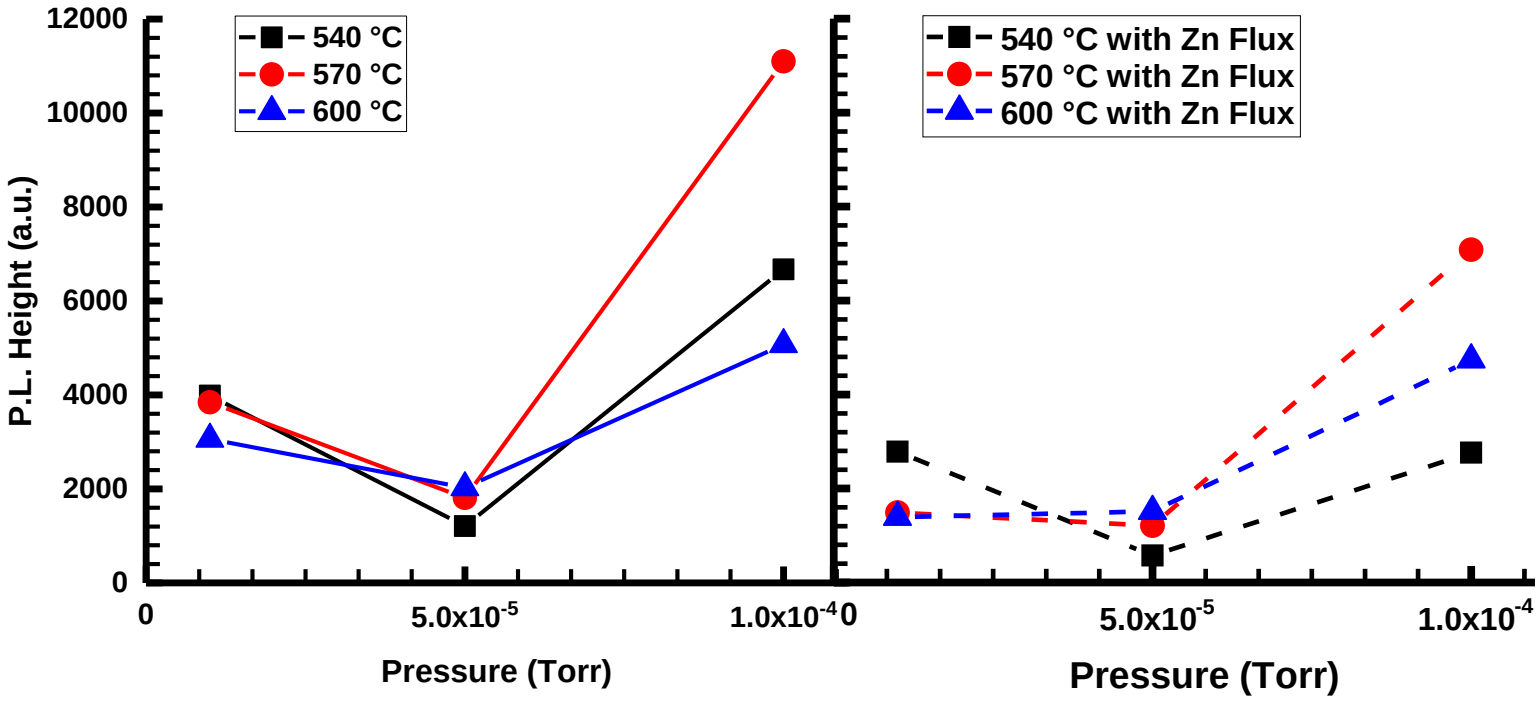

Figure 4.11 Pressure Dependence for 603 nm peak

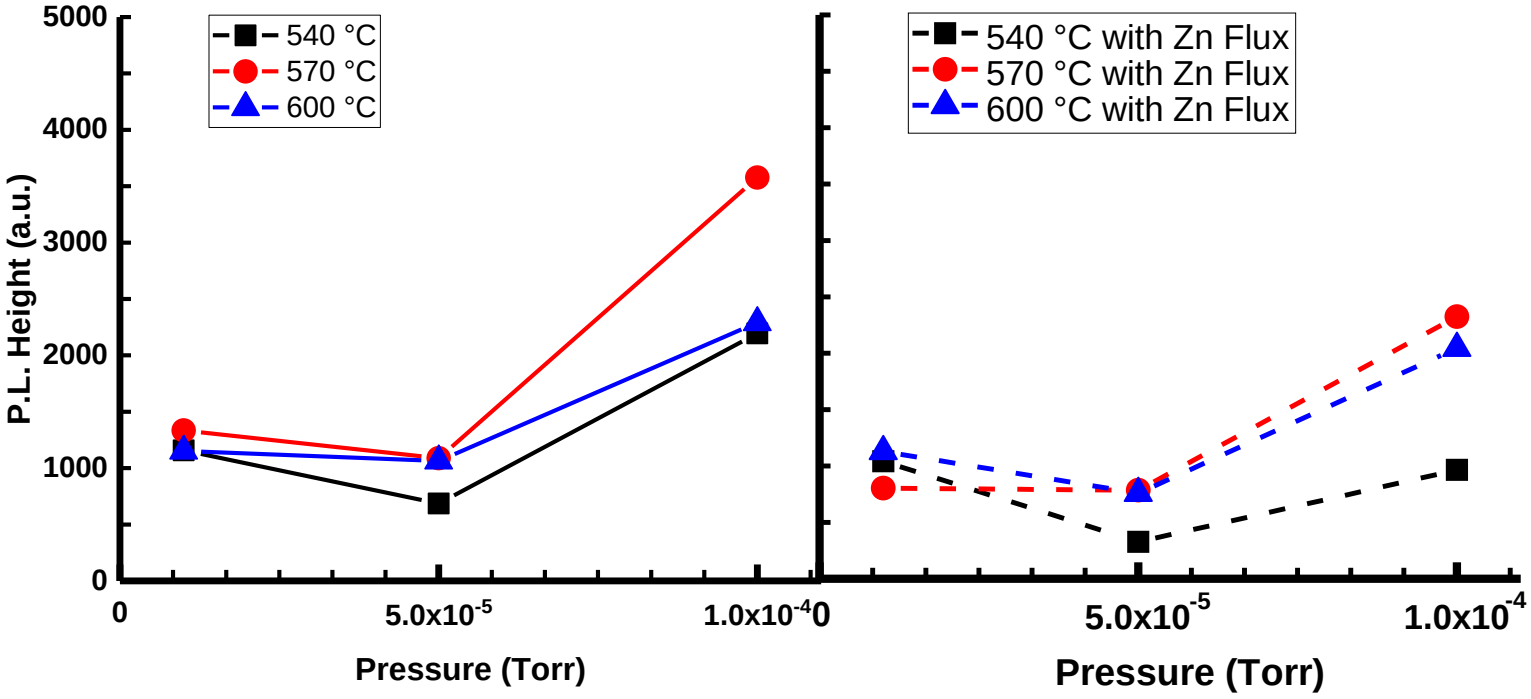

Figure 4.12 Pressure dependence for 650 nm peak

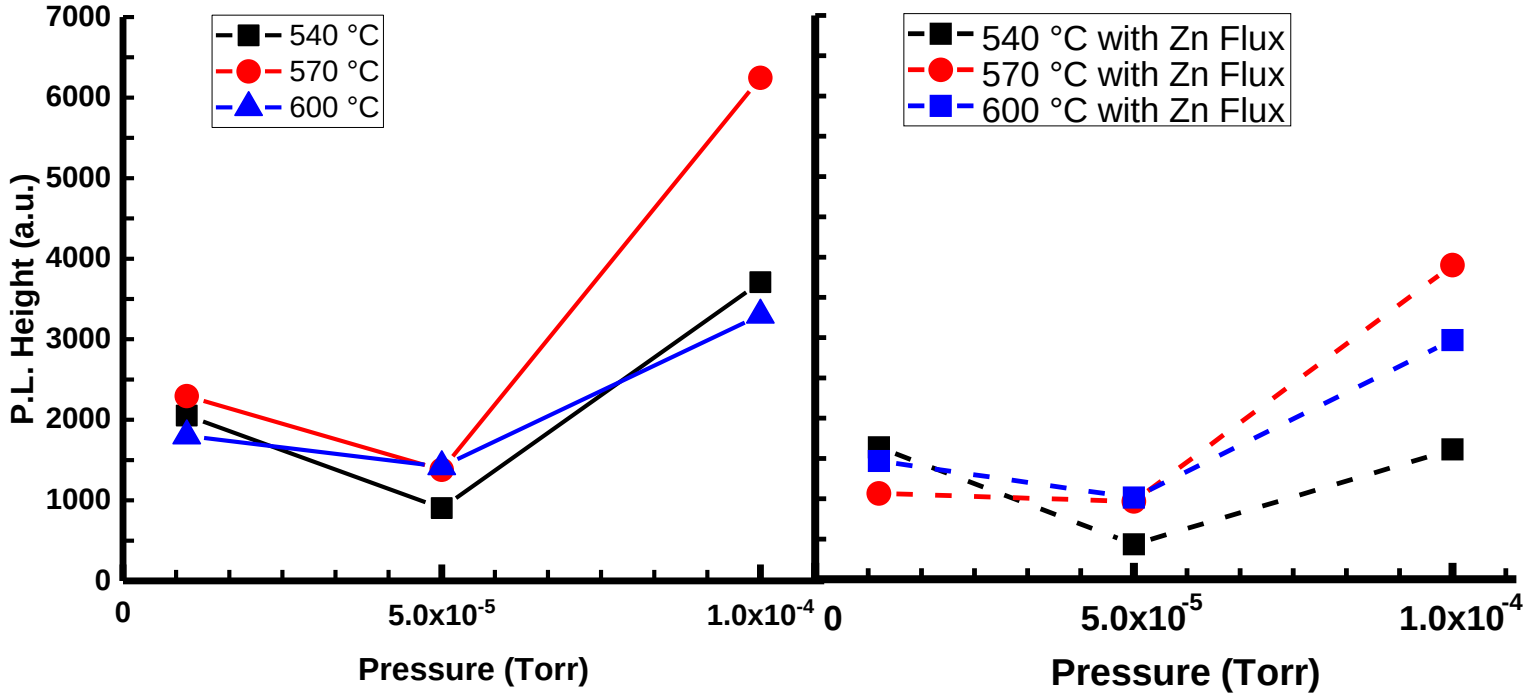

Figure 4.13 Pressure dependence for 675 nm peak

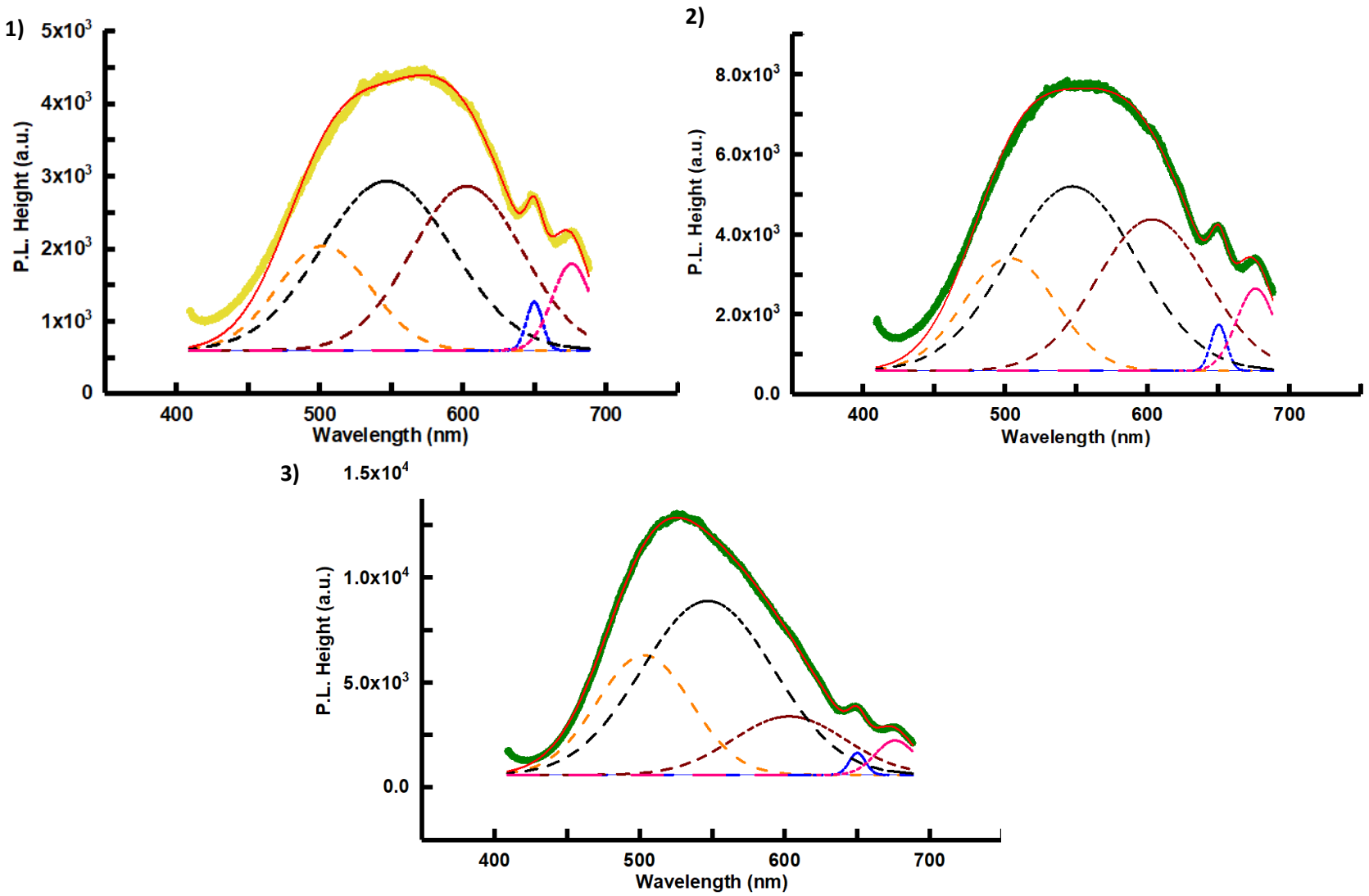

Figure 4.14 Gaussian fitted PL spectra for sample 1) As-received 2) Annealed under 540 ˚C 1×10^{-4} torr pure oxygen pressure 3) Annealed under 540 ˚C 1×10^{-4} torr pure oxygen pressure with Zn flux

4.7 References

[1] H. Hang, IEEE ELECTRON DEVICE LETTERS, VOL. 30, NO. 10, OCTOBER 2009

[2] D. C. Look, Mater. Sci. Eng. B, vol. 80, no. 1–3, pp. 383–387, Mar. 2001

[3] Y. Chen *et al.*, Mater. Sci. Eng. B, vol. 75, no. 2/3, pp. 190–198, Jun. 2000

[4] X.L. Wu, Appl. Phys. Let., Vol 78 (16) 2001

[5] S. C. Lyu, Chem Phys Let. Vol 363 (2) 2002

[6] K. Vanheusden, J. Appl. Phys, 79 7983 (1996)

[7] Y.G. Wang, J Appl. Phys, 94 (2003)

[8] A. Janotti, Rep. Prog. Phys. 72 (2009) 126501

[9] M. Willander *et al.*, *Materials*, 3(4) (2010)

[10] M. Li, PhD Thesis 2016

[11] P. Gorai, PhD Thesis, 2014

[12] K. L. Gilliard, PhD Thesis, 2017

[13] E. Seebauer *et al.*, Phys. Rev. Lett. 97 (2006) 055503.

[14] A. Hollister *et al.*, Appl. Phys. Lett. 102 (2013) 231601

[15] T. M. Borseth, Appl. Phys. Let., Vol 89, 262112 (2006)

[16] A. Janotti, and C. G. Van de Walle, Rep. Prog. Phys. **72** (2009)

[17] R. Helbig, J. Cryst. Growth **15** (1972), 25

[18] A. Janotti and C. G. Van de Walle, Phys. Rev. B **75**, 165202 (2007)

[19] S. G. Koch *et al.*, Phys. Rev. B **90** (2014), 205212

[20] X. Xue *et al.*, Cryst. Eng. Comm **16** (2014), 1207

[21] K. Vanheusden *et al.*, J. Appl. Phys **79** (1996), 7983

[22] F. H. Leiter *et al.*, Phys. Stat. Sol. **B 226** (2001)

[23] D. M. Hofmann *et al.*, Appl. Phys. A **88** (2007), 147-151

[24] Y. W. Heo, D. P. Norton, and S. J. Pearton, J. Appli. Phys **98**, 073502 (2005)

[25] T. Moe Børseth *et al.*, Appl. Phys. Lett. **89** (2006), 262122

[26] M. Liu, A. H. Kitai, and P. Mascher, J. Lumin. 54, 35 (1992)

[27] L. E. Greene *et al*., Angew. Chem. Int. Ed. **42** (2003), 3031-3034

[28] L. S. Vlasenko *et al.*, Phys. Rev. B **71** (2005), 125210

[29] L. A. Kappers *et al.*, Nucl. Instrum. Methods Phys Res. **266** (2008), 2953

[30] J. Lv *et al.*, Appl. Phys. Lett. **103** (2013), 232114

[31] A. L. *Taylor et* al., Solid State Commun. **8** (1970), 1359

[32] A. Janotti *et al*., Nature Mater. **6** (2007), 44

[33] X. Liu *et al.*, J. Appl. Phys **95** (2004), 6

[34] J. S. Kang *et al*., Thin Solid Films **443** (2003), 5-8

[35] T. Li *et al.*, J. Phys. D: Appl. Phys. **45** (2012) 185102

[36] K. E. Knutsen *et. al.*, Phys. Rev. B 86, 121203 (2012)

[37] C. Chandrinou *et al*, Microelectron. J. **40** (2009) 296-298

[38] A. Dev *et al*., Nanotechnology **21** (2010), 065709

[39] C. H. Ahn *et.al*., J. Appl. Phys., 105, 013502 (2009)

[40] C. Lin *et al.*, Appl. Phys. Lett. **86** (2005), 183103

[41] M. Kim *et al.*, *Solid. State. Commu.* **151** (2011), 768-770

[42] Y. H. Leung *et al.*, Appl. Surf. Sci. **271** (2013), 202-209

[43] K. H. Tam *et al*., J. Phys. Chem. B **110** (2006), 20865-20871

[44] N. Y. Garces *et al*., Appl. Phys. Lett. **81** (2001)

[45] A. Ortiz *et al*., Thin Sloid Films **293** (1997), 103-107

[46] P. Gorai *et al.*, ECS J. Solid. State. Sci. Technol. 1 (2012)

[47] Y. Li *et al.*, Appl. Phys. Lett. **76** (2000), 2011

[48] Y. W. Wang *et al.*, J. Cryst. Growth. **234** (2002), 171-175

[49] J. Yang *et al.*, International J. Mater. & Product. Tech. **34** (2009), 360

[50] H. Chen *et al.*, J. of Luminescence **131** (2011), 1189

[51] N. Ohashi *et al.*, Appl. Phys. Lett. **80** (202)

[52] G. Brauer *et al.*, Phys. Rev. B **79** (2009), 115212

[53] C. Ton-That, Phys. Rev. B, Vol 86, 115205 (2012)

[54] M. Li *et al.*, J. Phys. Chem. C 120 (2016)

[55] H. Nahm et al., *Sci. Rep*. (2014) 04214

[56] F. Oba *et al.*, Phys. Rev. B **77**, (2009) 245202

[57] S.A.M Lima *et al.*, Int. J. Inorg. Mate. **3** (2001) 749-754

[58] R. Gunawan *et al.*, J. Electrochem. Soc. **150**, (2003) G758

[59] K. L. Gilliard *et al.*, J. Phys.: Condensed Matter **29**, 44 (2017)

[60] F. Friedrich *et al.*, Appl. Phys. Lett. **95** (2009), 141903

[61] S. Pal *et al*, J. Phys. D: Appl. Phys. **51** (2018), 105107

[62] Yu. V. Gorelkinskii and G. D. Watkins, Phys. Rev. B **69**, (2004) 115212

[63] C. Cos¸kun *et al.*, Semicond. Sci. Technol. **19**, 752 (2004)

[64] N.O. Korsunska *at al.*, J. Lumin. **733** (2003) 102-103

[65] X. L. Xu *et al.*, J. Cryst. Growth **223** (2001) 201

[66] A. B. Djuriši *et al.,* Nanotechnology **18** (2007) 095702

[67] P. F. Carcia *et al.*, Appl. Phys. Lett. **82** (2003), 1117

[68] L. Wu *et al*., Opt. Mater. **28** (2006), 418

[69] E. V. Lavrov *et* al., Phys. Rev. B **79**, (2009) 165210

[70] X. L. Wu *et al.*, Appl. Phys. Lett. 78, 2285 (2001)

[71] M. Li *et al*., J. Phys. Chem. C **122** (2018), 2127-2136

[72] B. Lin *et al*., Appl. Phys. Lett. **79** (2001)